Astrobiology, research article

Cite this article as:
Dannenmann, M., Klenner, F., Bönigk, J., Pavlista, M., Napoleoni, M., Hillier, J., Khawaja, N., Olsson-Francis, K., Cable, M.L., Malaska, M.J., Abel, B., and Postberg, F. (2023) Toward Detecting Biosignatures of DNA, Lipids and Metabolic Intermediates from Bacteria in Ice Grains Emitted by Enceladus and Europa. *Astrobiology* **23**:in press.

Toward Detecting Biosignatures of DNA, Lipids and Metabolic Intermediates from Bacteria in Ice Grains Emitted by Enceladus and Europa

Marie Dannenmann[1,2,*], Fabian Klenner[1,*,#], Janine Bönigk[1,*], Miriam Pavlista[1,*], Maryse Napoleoni[1], Jon Hillier[1], Nozair Khawaja[1], Karen Olsson-Francis[3], Morgan L. Cable[4], Michael J. Malaska[4], Bernd Abel[5,6], Frank Postberg[1]

[1]Institute of Geological Sciences, Freie Universität Berlin, Berlin, Germany

[2]Department of Plant and Microbial Biology, University of Zurich, Zurich, Switzerland

[3]AstrobiologyOU, Faculty of Science, Technology, Engineering & Mathematics, The Open University, Milton Keynes, United Kingdom

[4]Jet Propulsion Laboratory, California Institute of Technology, Pasadena, CA, USA

[5]Leibniz-Institute of Surface Engineering (IOM), Leipzig, Germany

[6]Wilhelm-Ostwald-Institute for Physical and Theoretical Chemistry, Leipzig University, Leipzig, Germany

[*]These authors contributed equally to this work.

[#]Corresponding author e-mail: f.klenner@fu-berlin.de

Submitted: 2022 May 17. Accepted for publication: 2022 September 14.

Abstract

The reliable identification of biosignatures is key to the search for life elsewhere. On ocean worlds like Enceladus or Europa this can be achieved by impact ionization mass spectrometers, such as the Surface Dust Analyzer (SUDA) on-board NASA's upcoming Europa Clipper mission. During spacecraft flybys, these instruments can sample ice grains formed from subsurface water and emitted by these moons. Previous laboratory analogue experiments have demonstrated that SUDA-type instruments could identify amino acids, fatty acids and peptides in ice grains, and discriminate between their abiotic and biotic origins. Here we report experiments simulating impact ionization mass spectra of ice grains containing DNA, lipids, and metabolic intermediates extracted from two bacterial cultures: *Escherichia coli* and

***Sphingopyxis alaskensis*. Salty Enceladan or Europan ocean waters were simulated using matrices with different NaCl concentrations. Characteristic mass spectral signals, such as DNA nucleobases, are clearly identifiable at ppm-level concentrations. Mass spectra of all substances exhibit unambiguous biogenic patterns, which in some cases show significant differences between the two bacterial species. Sensitivity to the biosignatures decreases with increasing matrix salinity. The experimental parameters indicate that future impact ionization mass spectrometers will be most sensitive to the investigated biosignatures for ice grain encounter speeds of 4-6 km/s.**

Keywords: Space missions, LILBID, Analogue experiments, Extraterrestrial life, Mass spectrometry, Icy moons

1 Introduction

Enceladus and Europa, icy moons of Saturn and Jupiter, respectively, host global, subsurface, liquid water oceans (Hoppa et al., 1999; Thomas, 2016). A plume has been detected on Enceladus (Hansen et al., 2006; Porco et al., 2006; Spencer et al., 2006), ejecting gas and water ice grains formed from the moon's global subsurface ocean into space. Similar phenomena may occur on Europa (Roth et al., 2014; Sparks et al., 2016; Jia et al., 2018). The presence of water, combined with the

availability of energy and chemical disequilibrium (Hand et al., 2007) make these moons compelling places to search for life in the outer solar system as these oceans provide potential habitable environments (Russell et al., 2014; Cockell et al., 2016). We define life here and throughout the paper as life as we know it to exist on Earth, based on organic chemistry and water.

The emitted ice grains can be sampled *in situ* during spacecraft flybys using impact ionization mass spectrometers, such as the Cosmic Dust Analyzer (CDA; Srama et al., 2004) on-board the past Cassini mission, the SUrface Dust Analyzer (SUDA; Kempf et al., 2014), which is being built for NASA's upcoming Europa Clipper mission (Howell and Pappalardo, 2020) and the Enceladus Ice Analyzer (ENIA; Srama et al., 2015), which is proposed for future Enceladus missions (Reh et al., 2016; Mitri et al., 2018). Impact ionization mass spectrometers thereby provide a cost-effective means of assessing the physical and chemical properties – and thus, habitability – of the moons' subsurface oceans. Hypervelocity ($\geq$ 1 km/s) impacts of nm- to µm-sized ice grains onto the ionization mass spectrometer's metal target generate ions, which are then separated by an electric field, eventually producing time of flight (TOF) mass spectra (e.g., Srama et al., 2004). Due to the impact ionization process creating almost exclusively singly charged ions, the spectral peak positions, i.e., ion arrival times at the detector, therefore depend only on the ions' masses. While CDA was sensitive only to cations, SUDA and ENIA will be capable of producing both cation and anion mass spectra.

For a detailed spectral analysis, terrestrial calibration experiments are needed. Although the acceleration of siliceous and organic particles is feasible up to 10 s of km/s (e.g., Bowden et al., 2009; Hillier et al., 2009; Srama et al., 2009; Burchell et al., 2014; Hillier et al., 2018; New et al., 2020; Fisher et al., 2021; Kazemi et al., 2021), the controlled acceleration of µm-sized ice grains in a laboratory environment is extremely technically challenging (e.g., Belousov et al., 2021). However, a technique employing Laser Induced Liquid Beam Ion Desorption (LILBID), which was introduced by Brutschy et al. (Kleinekofort et al., 1996a; Kleinekofort et al., 1996b) and applied to the analysis of large biomolecules by Abel and co-workers (Charvat and Abel, 2007), has been further developed to accurately reproduce mass spectra generated by impact ionization of ice grains impacting the detectors' metal targets at relevant speeds varying from 2 to > 20 km/s (Klenner et al., 2019). In addition to speed-dependent, non-compositional differences, this technique has successfully been used to infer compositional differences of ice grains emitted by Enceladus from Cassini mission spectra obtained by CDA (e.g., Postberg et al., 2009, 2011, 2018a; Khawaja et al., 2019).

Comparing the analog laser desorption laboratory data with CDA mass spectra revealed that Enceladus' ocean is salty, with sodium salts being the most abundant non-water compounds at a total concentration of 0.05 – 0.2 M (Postberg et al., 2009) and contains a variety of organic compounds (Postberg et al., 2008; Postberg et al., 2018a; Khawaja et al., 2019). In fact, ~25 % of Enceladan ice grains contain organic

material at detectable concentrations (Postberg et al., 2008; Postberg et al., 2018b). Volatile low-mass oxygen- and nitrogen bearing compounds have been identified in the majority of these organic-enriched ice grains (Khawaja et al., 2019), while 5-10 % of these grains (1.25 - 2.5 % of the total ice grains emitted by Enceladus) contain even more complex, refractory macromolecules at concentrations ≥ 0.5 % wt. (Postberg et al., 2018a). The volatile organics are thought to be previously dissolved in Enceladus' ocean and, subsequently, their high vapor pressures enable sufficient evaporation from the subsurface water. These initially gaseous organics undergo condensation and adsorption onto water ice nucleation cores during ascent in Enceladus' ice vents (Bouquet et al., 2019; Khawaja et al., 2019). In contrast, the refractory, probably hydrophobic, macromolecules are believed to originate from a thin organic layer floating on top of Enceladus' subsurface water table (Postberg et al., 2018a). However, despite the detection of even macromolecular of organic compounds, it is still unclear whether Enceladan ice grains contain biosignatures or even remnants of microbial life forms.

LILBID experiments have also been used to predict the mass spectral appearances and detection limits for ice grain detections of abiotic organics as well as those of potential biosignatures by a SUDA-type instrument (Klenner et al., 2020a, 2020b). Klenner et al. (2020a) conducted LILBID experiments with amino acids, fatty acids and peptides and concluded that these biologically important molecules would be detectable down to the ppb level using impact ionization mass spectrometry.

Characteristic abiotic and biotic fingerprints of these molecules could be reliably discriminated from each other in mass spectra of salt-poor as well as in those of salt-rich ice grains (Klenner et al., 2020b). Impact ionization instruments on spacecrafts appear to be most sensitive to these delicate molecules enclosed in the ice grains and their characteristic mass spectral signals emerging from impacts of the particles on the detector at encounter velocities of 4-6 km/s (Klenner et al., 2020b). Theoretical simulations by Jaramillo-Botero et al. (2021) support this speed regime. According to these simulations, encounter velocities of 3-5 km/s are ideal for the detection of bare amino acids and fatty acids while 4-6 km/s appears to be an optimal speed window for the identification of the same species when they are enclosed in ice grains (Jaramillo-Botero et al., 2021). Slightly higher speeds of 7 - 10 km/s would allow for the predominant formation of potentially characteristic fragment ions while the parent molecular signatures become less apparent. While informative, these experiments involved commercially available chemicals (either pure or in mixtures); the next step is to validate impact induced ionization analyses with samples of true biotic origin.

Building on the preliminary findings, we investigate, with the same laboratory laser desorption setup, mass spectra of deoxyribonucleic acid (DNA), lipids and hydrophilic cell compounds extracted from bacterial cells. We have chosen two different bacterial species for our investigations: *Escherichia coli* and *Sphingopyxis alaskensis*, formerly described as *Sphingomonas alaskensis*. *E. coli*, as the most

widely studied free-living organism on Earth, is a facultative anaerobic bacterium with an optimal reproduction temperature at 37 °C and a rapid growth rate, thus able to adapt relatively fast to moderate changes in environmental conditions (e.g., Taj et al., 2014). *S. alaskensis* is a psychrophilic organism that has been isolated from various marine environments (e.g., Schut et al., 1993; Schut et al., 1997; Eguchi et al., 1996). Some strains can grow at temperatures below 5 °C (Eguchi et al., 2001). This ultramicrobacterium (volume of < 0.1 μm^3), small enough to be potentially enclosed within the µm-sized Enceladan ice grains, can utilize low concentrations of nutrients, and thus grow in oligotrophic environments that provide only a very low nutrient flux (Poindexter, 1981; Cavicchioli et al., 2003). This organism therefore may be more representative of putative life in Enceladus' ocean.

DNA is used by life forms on Earth to store genetic information. In its most basic structure, DNA forms a double helix containing four nucleobases (adenine, guanine, cytosine, thymine), stabilized by a phosphate-deoxyribose backbone. The nucleobases are classified into purines (adenine, guanine) and pyrimidines (cytosine, thymine), with adenine always binding to thymine and guanine always binding to cytosine (Frankling and Gosling, 1953; Watson and Crick, 1953; Wilkins et al., 1953). Thus, an equal ratio of adenine to thymine and guanine to cytosine, respectively, can be considered a characteristic trait of DNA deriving from terrestrial life. However, modified nucleobases can occasionally be found in DNA,

such as the pyrimidine base uracil, which derives from deamination (removal of NH_2) of cytosine and replaces thymine in the DNA structure (Krokan et al., 2002; Kumar et al., 2018). Although individual nucleobases can form abiotically, for example through dehydration and condensation of formamide (Hudson et al., 2012), DNA is known to form only through biological processes and therefore detection of DNA in an extraterrestrial environment has the potential to provide unambiguous evidence for life beyond Earth. In fact, the complexity of such biopolymers, produced by living organisms, is one of the most direct signs of extant or extinct life (Summons et al., 2008; Davila and McKay, 2014).

Lipids are the main components of cell membranes in terrestrial life forms (e.g., Singer and Nicholson, 1972), with glycerophospholipids being most abundant in bacterial membranes (e.g., López-Lara and Geiger, 2017). These glycerophospholipids consist of a phosphate ester binding to the glycerol moiety, thereby forming a polar head group, with hydrophobic fatty acids of various length binding to the glycerol (e.g., Duncan et al., 1971). Fatty acids are biochemically produced by the addition of two carbon atoms at a time, which results in an excess of even numbered carbon atoms fatty acids when examining unbranched and saturated fatty acids, with hexadecanoic acid (C_{16}) and octadecanoic acid (C_{18}) dominating (Georgiou and Deamer, 2014). This excess of saturated even carbon number fatty acids can serve as a biosignature resulting from the biological synthetic pathways and could, in fact, be discriminated from abiotically produced

fatty acid abundance patterns using impact ionization mass spectrometry in space (Klenner et al., 2020b). These fatty acid abundance patterns may be less apparent in thermophilic and psychrophilic organisms (like *S. alaskensis*) as changing the ratio of saturated to unsaturated fatty acids is a common adaptive method to maintain membrane structure and flexibility at extreme temperatures (Langworthy, 1982; Wirsen et al., 1986).

Of particular relevance to impact ionization mass spectrometry are the effects of ocean constituents other than water on the spectral appearance and detection limits of biosignatures. A large fraction of Enceladan ice grains is frozen ocean spray, with sodium salts (chlorides and carbonates) representing the dominant non-water constituents (~1 % by mass; Postberg et al., 2009). Endogenous sodium and magnesium salts are believed to exist on Europa's surface (Brown and Hand, 2013; Ligier et al., 2016; Trumbo et al., 2019). Upon impact ionization, large quantities of cations and anions are produced by these salts and may suppress the spectral signals of other compounds (e.g., Annesley, 2003; Piwowar et al., 2009). For example, Klenner et al. (2020b) observed that in LILBID experiments the sensitivity to amino acids drops by a few orders of magnitude when they are measured in 1% NaCl solutions. Sodiated molecules represented the characteristic spectral amino acid signals, in contrast to protonated/deprotonated molecules that are observed in spectra of amino acids in salt-poor aqueous solutions.

On Earth, 70% of the planetary surface is covered by a biofilm, namely the surface microlayer on top of the ocean water (Flemming and Wuertz, 2019). It is an important link for exchange processes between hydrosphere and atmosphere and hosts a distinct microbial community, the 'bacterioneuston', at cell densities 3 – 5 orders of magnitude higher than in the bulk water phase (Bezdek and Carlucci 1972; Franklin et al., 2005). After death, oceanic bacterial cells decompose over time into smaller, hydrocarbon-based cell components. These decomposition products reside in the organic biofilm e.g., serving as food for living organisms (Waksman and Carey, 1933), or dissolve in the bulk water phase. Analogous, bacterial decomposition products on Enceladus or Europa may be expected to either stay in a separate organic layer/biofilm at the upper ice-water interface or be dissolved in the bulk water phase. Bacterial lipids and fatty acids are poorly water soluble and are not expected to be significantly dissolved in a cold (~ 0 °C) salty water ocean and, instead, may stay in the separate organic layer/biofilm. After aerosolization at the base of an Enceladan conduit, these compounds can serve as nucleation cores for water vapor, thereby forming salt-poor ice grains in the plume (Postberg et al., 2018a). Hence, we measure extracted lipids in salt-poor background solutions. In contrast, hydrophilic compounds, such as DNA or amino acids (protein fragments or bacterial metabolites), are more water soluble and thus may not only be present in an organic biofilm but can also dissolve in the salty ocean water. We therefore

investigate extracted DNA and the hydrophilic cell compounds in both salt-poor matrices as well as matrices with increasingly high sodium salt concentrations.

2 Methods

Mass spectra were recorded using the LILBID technique. Here, the experimental setup as well as the preparation of the biosignature solutions are described.

2.1 Experimental

The experimental setup used for this work (Figure 1) is described in detail in Klenner et al., (2019) and, as such, we only provide a brief overview here.

The impact ionization process was replicated by irradiating a µm-sized liquid water beam with a pulsed (20 Hz, 7 ns pulse length) infrared laser at variable laser energies. A flashlamp energy of 5.40 J and wavelength of 2840 nm were selected to excite the OH-stretch vibration of the water molecules. The water beam absorbs the laser energy and, on each pulse, thermally explodes into charged and uncharged atomic, molecular and macroscopic fragments (Charvat and Abel, 2007; Wiederschein et al., 2015). The resulting charged cations or anions (dependent on the instrument's polarity) are accelerated through two electrodes (Figure 1) and analyzed in a Time-of-Flight (TOF) mass spectrometer. The mass spectrometer uses the principle of delayed extraction (Klenner et al., 2019). Setting a predefined

delay time between laser shot and switch on of the acceleration electrodes allows the extraction of the ions as a function of their initial velocities.

The detected signals are pre-amplified, digitized and subsequently generate a TOF mass spectrum, recorded with a LabVIEW-controlled computer. The mass spectra presented here are typically an average of 300 – 500 individual spectra, co-added to improve the signal-to-noise ratio to a level that represents a spectrum of a single µm-sized ice grain recorded by a SUDA-type instrument. The recorded mass spectra (cations and anions) typically have a mass resolution of 600 – 800 m/Δm (full width at half maximum). At least 0.3 mL of sample volume are needed for one effective measurement. To ensure reproducibility, the experimental setup is calibrated at the beginning of each measurement day using a 10^{-6} M NaCl solution at three different delay time-laser intensity settings.

All spectra recorded with the LILBID setup were archived in a comprehensive spectral database and can be compared to past and future impact ionization data recorded in space (Klenner et al., under review).

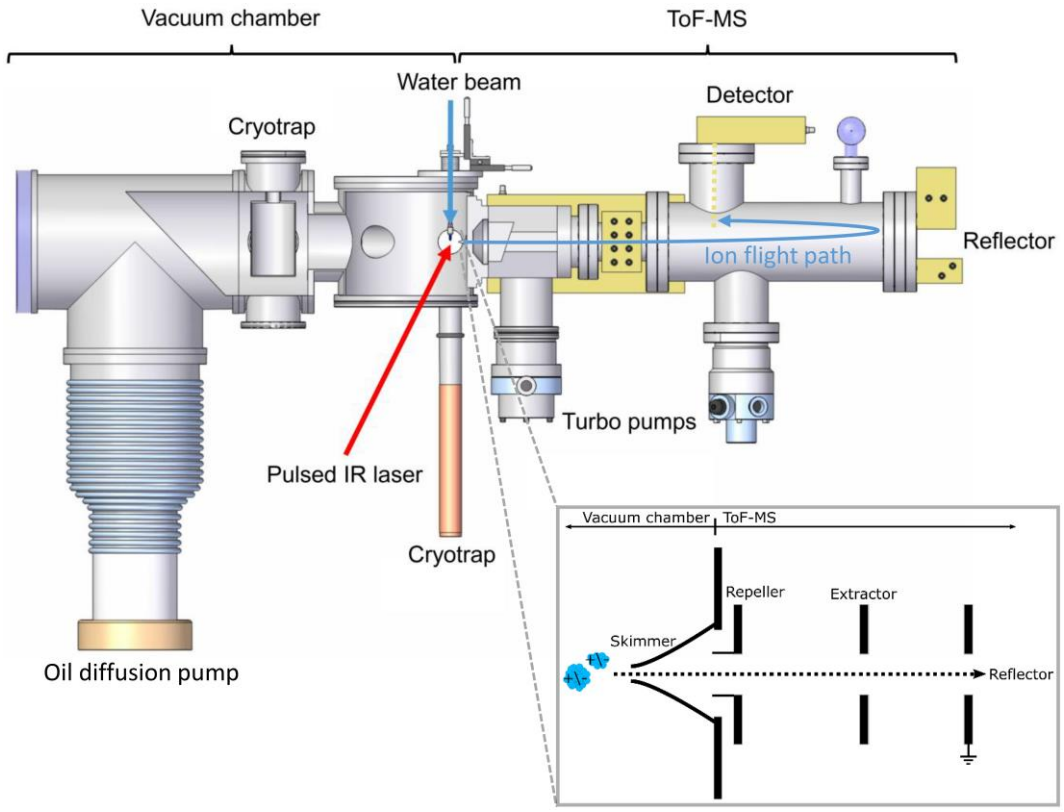

Figure 1: Laboratory setup for simulating mass spectra generated by ice grains impacting the plate of an impact ionization mass spectrometer in space (reproduced from Klenner et al., 2019). The inset on the bottom right shows the principle of delayed extraction. The oil diffusion pump shown has recently been replaced by a turbomolecular pump.

2.2 Preparation of biosignature solutions

E. coli cells (strain W3110) were cultured at the Institute of Biology and the Institute of Experimental Physics, Freie Universität Berlin. The cultures were

grown overnight in Lysogney Broth (LB) medium (Bertani, 1951) at 37 °C. Cells were harvested in 1 mL aliquots and washed twice with 0.9% NaCl by centrifugation at 16,000 × g for one minute (Model Biofuge pico, Kendro Laboratory Products). The cell material was stored as pellets at -20 °C until use. *S. alaskensis* (strain DSM 13593) was cultured at the Faculty of Science, Technology, Engineering & Mathematics, The Open University, UK. Cultures were grown overnight at 29 °C in Tryptone Soya Broth (TSB) (MacFaddin, 1985) medium. Cells were harvested and washed three times with 0.9% NaCl by centrifugation (12,000 × g, for 10 min). The cell material was air-desiccated and stored at -20 °C until use.

Using the *E. coli* and *S. alaskensis* cells, three main fractions (DNA, lipids, hydrophilic compounds) have been investigated using five different types of salt-poor or salt-rich solutions: i, ii, iii, iv, v (Table 1, described below).

2.2.1 Bacterial DNA in salt-poor (solution type i) and salt-rich (solution type ii) solutions

DNA of *E. coli* was extracted using the Norgen Biotek Bacterial Genomic DNA Isolation Kit, as per manufacturer's instructions. The Elution buffer B provided in the kit for elution of the DNA after it is bound to the spin column contains Tris-Hydrochloride (Tris-HCl) and Ethylenediaminetetraacetic acid (EDTA). Traces of

both chemicals could remain in the DNA samples, potentially resulting in strong mass lines in the recorded mass spectra. To avoid these signals, which could interfere with characteristic DNA signals, Elution buffer B was substituted with Milli-Q H_2O to elute the DNA from the spin column. To optimize the DNA yield, the elution step was repeated. This increased DNA yield (200-250 ppmw as opposed to ~50 ppmw).

The Norgen Biotek Bacterial Genomic DNA method did not yield sufficient DNA with *S. alaskensis*; hence the Genomic DNA Purification Kit from ThermoFisher (K0512) was used, as per manufactures instructions. The kit is based on a selective detergent-mediated DNA precipitation method. Chloroform is added to the *S. alaskensis* cell lysate (10 mg dry weight) to produce a biphasic system. Following separation, the DNA is then precipitated from the aqueous phase and washed with cold ethanol before dissolution in deionized water, yielding DNA extracts of 3-4 ppmw.

DNA concentrations were measured with either a NanoDrop 2000c (ThermoFisher Scientific) photometer or a Quantus™ Fluorometer (Promega). The DNA samples were stored at -20 °C until further use.

Following the above-described procedures, genomic DNA was obtained in a salt-poor matrix (solution type i.). To account for the effects of a salty Enceladan or Europan ocean, the DNA was prepared in NaCl solutions over a range of

concentrations (10^{-5} M, 10^{-4} M, 10^{-3} M, 10^{-2} M, and 10^{-1} M NaCl), representing solution type ii.

2.2.2 Bacterial lipids in salt-poor solutions (solution type iii)

Lipids were extracted using a chloroform-methanol-based isolation method, initially developed by Bligh and Dyer (1959) and modified for bacterial samples (e.g., Ames, 1968). Lipids were extracted from frozen ~ 10^9 cells using a solvent mixture of H_2O, methanol and chloroform (4:10:5). Samples were mixed by inversion and incubated for 10 minutes at 4 °C, after which equal volumes (1 mL each) of chloroform and H_2O were added. To complete separation of the lipids and the aqueous phase, the samples were centrifuged at 3000 $\times$ g for 15 minutes (Heraeus Megafuge 16, ThermoFisher Scientific), forming a biphasic system with an interphase. The chloroform-lipid phase (lowest layer) was obtained by pipetting. The volatile chloroform was evaporated with an air stream and the lipids remained in the sample tube. Due to the lipids' poor solubility in water, pure H_2O was found to be unfeasible for dissolving these organics and a mixture of 10 mL H_2O and 20 mL isopropanol was used instead. The lipid samples (solution type iii) were either immediately used for LILBID analysis or stored in the refrigerator at 7 °C until further use.

2.2.3 Hydrophilic cell compounds in salt-poor (solution type iv) and salt-rich (solution type v) solutions

Following addition of H_2O and chloroform to the cells, the biphasic system derived from the Bligh and Dyer (1959) lipid extraction contained an upper aqueous phase, a lower chloroform-lipid phase, and a clearly visible interface between these two phases. The aqueous phase contains polar, hydrophilic molecules, such as amino acids, sugars, or DNA from ~10^9 cells dissolved in a water-methanol matrix (see section 2.2.2). These samples (solution type iv) were stored at 7 °C until further use. To account for the effects of a salty extraterrestrial ocean, we added different concentrations of NaCl (10^{-4} M, 10^{-2} M, and 10^{-1} M) to the hydrophilic cell compounds (solution type v).

Table 1 *Biosignature solutions*

Type	**Cell compound**	**Added NaCl concentrations**
i	DNA – salt poor	0 M
ii	DNA – salt rich	10^{-5} M, 10^{-4} M, 10^{-3} M, 10^{-2} M, and 10^{-1} M
iii	Lipids – salt poor	0 M
iv	Hydrophilic compounds – salt poor	0 M
v	Hydrophilic compounds – salt rich	10^{-4} M, 10^{-2} M, and 10^{-1} M

3 Results and Mass Spectral Analysis

3.1 DNA

In the mass spectra of DNA extracted from both bacterial species in pure water (solution i), identical spectral characteristics can be clearly identified, including nucleobases and fragments of the DNA´s phosphate-deoxyribose backbone. In the cation mass spectrum of the DNA (Figure 2), protonated cytosine (m/z 112), adenine (m/z 136), and guanine (m/z 152) are clearly identifiable. The fourth nucleobase thymine can be tentatively identified (m/z 127), but this peak interferes with a cluster peak from the water matrix $(H_2O)_6H_3O^+$. Several nucleobase fragments are detected, such as [cytosine-HNCO]$^+$ (m/z 68), [adenine-2HCN]$^+$ (m/z 81), [guanine-NHCN]$^+$ (m/z 110), [thymine-CH3]$^+$ (m/z 111), and [adenine-NH_2]$^+$ (m/z 119). Protonated fragments of the phosphate-deoxyribose backbone of the DNA can also be identified, such as $[H_4PO_3]^+$ (m/z 83), $[H_4PO_4]^+$ (m/z 99), and protonated deoxyribose (m/z 135). Unlabeled peaks in all spectra are yet to be identified.

The base peak at m/z 60 might derive from the fragmentation of the amino acid serine ([Ser-COOH]+), or be attributed to protonated guanidine (i.e., the guanidinium cation $[HNC(NH_2)_2 + H]^+$), which could potentially be produced by the fragmentation of either guanine or arginine (Reiss et al., 2015; Zhang et al., 2020), or originate from guanidine hydrochloride used during the DNA extraction. Consequently, an additional DNA extraction method without the use of guanidine hydrochloride (the ethanol precipitation method, described in Supplementary

Information S1) was performed to evaluate the relative contribution of nucleobase fragments to the peak at m/z 60. The resulting cation mass spectrum of *E. coli* DNA (Figure S1, top panel) shows a high peak at m/z 60, demonstrating that DNA fragments significantly contribute to this peak.

In DNA anion spectra (Figure 3), we were still able to clearly detect three nucleobases (deprotonated thymine, adenine, and guanine) at DNA concentrations of 3 ppm (as opposed to ~100 ppmw in cation spectra), as well as PO_3^- (m/z 79), a characteristic fragment of the DNA's sugar backbone. The S/N (signal-to-noise ratio) of PO_3^- and adenine indicate a detection limit below 1ppm. The anion mode appears to be more sensitive to mass spectral signals of DNA than the cation mode.

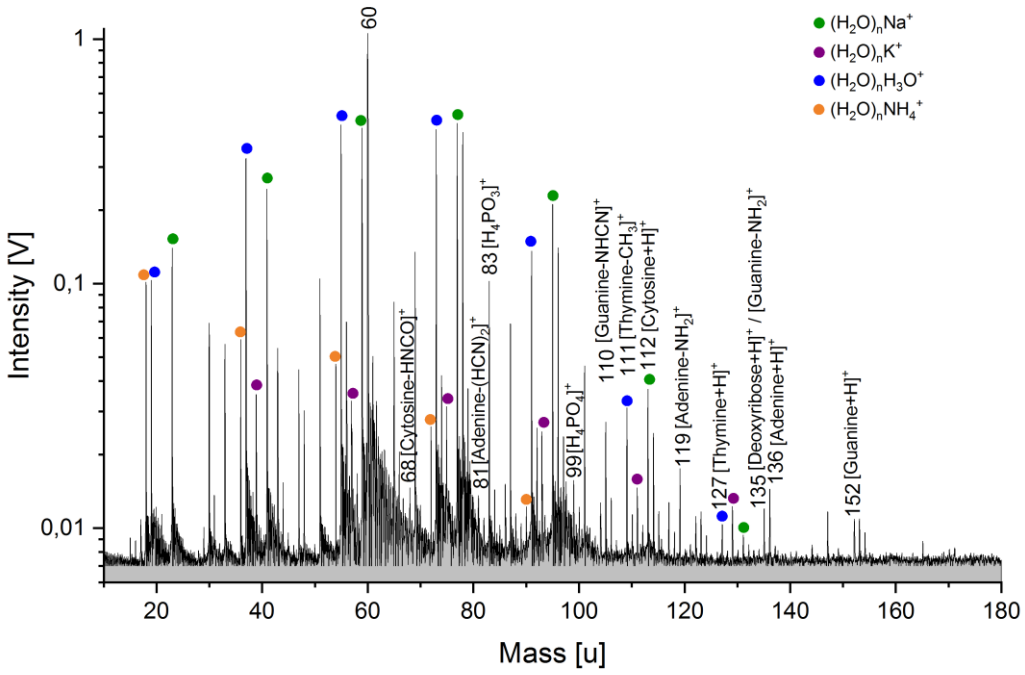

Figure 2: Baseline corrected cation mass spectrum (y-axis in logarithmic scale) of E. coli DNA (100-150 ppmw) in H_2O. Characteristic DNA fragments, such as protonated nucleobases (cytosine, adenine, and guanine), are observable. The mass spectrum was recorded at a delay time of 5.9 µs and a laser intensity of 98.1%.

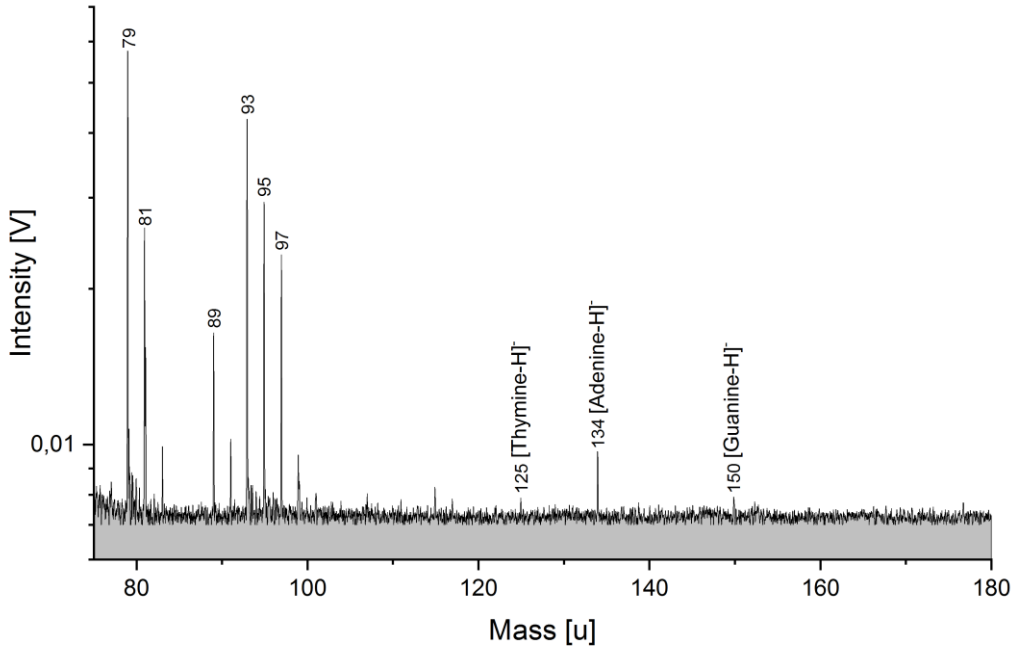

Figure 3: Section (m/z 75 – 180) of a baseline corrected anion spectrum (y-axis in logarithmic scale) of S. alaskensis DNA (3 ppmw) in H_2O. Characteristic DNA fragments, such as deprotonated nucleobases (thymine, adenine, and guanine) as well as phosphate from the DNA backbone are clearly observable. The mass spectrum was recorded at a delay time of 5.4 µs and a laser intensity of 100%.

The spectra of genomic DNA in salt-rich matrices (solution ii) show that biosignatures from the DNA can be identified even at relatively high salt concentrations: nucleobases can be detected in their deprotonated form in salt-rich background solutions at NaCl concentrations up to 0.01 M (Figure S2). The

experimental setup appears to be more sensitive to the two purine nucleobases (adenine and guanine) than to the pyrimidine nucleobases (cytosine and thymine). The sensitivity to the biosignature decreases with increasing salinity of the matrix due to suppression effects of the salt species on the biomolecules (Annesley, 2003; Piwowar et al., 2009; Klenner et al., 2020b).

3.2 Lipids

Bacterial lipids were measured in a water-isopropanol (1:2 v:v) matrix because of their poor solubilities in water (solution type iii). Isopropanol produces only few low-amplitude peaks at masses above ~120 u that can be well distinguished from the peaks derived from the analytes. Characteristic lipid fragments, i.e., fatty acids (saturated as well as unsaturated) and phospholipid fragments (Figure 4), strongly favor forming deprotonated molecular anions $[M-H]^-$ over protonated molecular cations $[M+H]^+$. Lipid samples were therefore only investigated in anion mode.

Deprotonated *n*-hexadecanoic acid (saturated C_{16} at m/z 255) and *n*-octadecanoic acid (saturated C_{18} at m/z 283) molecules produce the strongest signals from *E. coli* lipids while deprotonated *n*-pentadecanoic acid (saturated C_{15} at m/z 241), *n*-hexadecanoic acid and *n*-octadecanoic acid molecules form the strongest peaks from *S. alaskensis* lipids. With our setup we cannot distinguish between the unbranched and mono-methyl-branched fatty acids as they have the same molecular

mass. Thus, the fatty acids might also be present in their iso- or anteiso-methyl-branched form. However, we note that unbranched fatty acids have been found to be more abundant in *E. coli* and *S. alaskensis* than branched fatty acids and are, thus, more likely to represent the peaks in the spectra (e.g., Mejía et al. 1999; Kim et al. 2005; Choi et al., 2010). More saturated than unsaturated fatty acids can be observed from lipids of both bacterial species. Unsaturated fatty acids appear always together with the respective saturated fatty acids of the same number of carbon atoms, except saturated cyclo C_{17} at m/z 267 from *E. coli* lipids (Figure 4 top panel). This peak derives from 9,10-methylenehexadecanoic acid, which is particularly characteristic of *E. coli* (e.g., Oursel et al., 2007). Fatty acid dimers were not observed.

In the anion spectrum of *S. alaskensis* lipids, phosphatidylglycerol (PG) lipid fragments originating from the loss of one of its two fatty acids can be observed (Figure 4 bottom panel). The fragments derive either from the loss of one fatty acid acyl chain as ketene (RCH=C=O) and glycerol – m/z 353, m/z 395, and m/z 423 with the fragmented head group binding saturated C_{12}, C_{15}, and C_{18}, respectively – or neutral loss of one fatty acid acyl chain, its carboxyl group and glycerol from the lipid molecule resulting in peaks at m/z 377 and 391 from saturated C_{15} or C_{16}, respectively, binding to the head group derived phosphate compound.

To account for a low-intermediate salt concentration as might be expected in the organic layer on top of Enceladus' ocean from physical disruption, e.g., via bubbles

bursting, we added increasing concentrations of NaCl to the lipid samples. While peak amplitudes from all deprotonated fatty acids and phospholipid fragments decrease with increasing salt concentration, those of the strongest signals (m/z 255 and 283 from *E. coli* lipids and m/z 241, 255 and 283 from *S. alaskensis* lipids) are still clearly detectable when a NaCl concentration of 10^{-3} M is present.

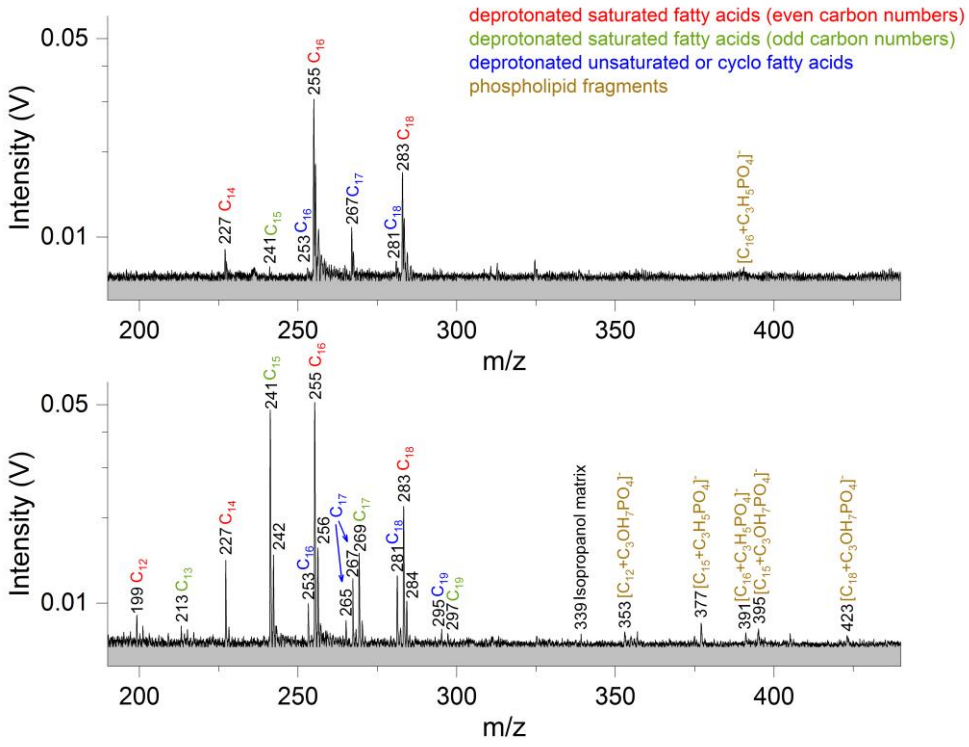

Figure 4: Sections (m/z 190 - 440) of two baseline corrected anion mass spectra (y-axis in logarithmic scale) of lipids extracted from ~10^9 E. coli cells (top panel) and ~10^9 S. alaskensis cells (bottom panel), respectively. Because of their poor

water solubilities, the lipids were dissolved in 30 mL water:isopropanol (1:2 vol; solution type iii). Peaks of deprotonated fatty acids as well as phospholipid fragments are observable, with saturated C_{16} and C_{18} showing the most prominent peaks for E. coli and saturated C_{15}, C_{16} and C_{18} being the most abundant species for S. alaskensis. Mass spectra of E. coli lipids and S. alaskensis lipids were recorded at delay times of 8.0 and 8.5 µs and laser intensities of 96.9 and 97.3 %, respectively.

3.3 Hydrophilic cell compounds

The samples containing hydrophilic cell compounds were measured without further dilution (solution type iv). In the resulting mass spectra (Figure 5 and 6), matrix peaks from water and methanol are observable. Cation and anion spectra of methanol:water (1:1 v:v) can be found in Figure S3. Sodium and potassium cations as well as chlorine anions from the cell's cytosol form prominent peaks in the mass spectra. A variety of metabolic intermediates, in particular amino acids, can be identified in the cation mode. Nucleobases (DNA fragments) and metabolic intermediates prevail in the anion mode.

The following amino acids can be assigned to their respective protonated peaks in the cation spectrum of the *S. alaskensis* hydrophilic compounds (Figure 5): serine (m/z 106), valine (m/z 118), and lysine (m/z 147). Alanine (m/z 90), serine, valine,

threonine (m/z 120), and asparagine (m/z 133) can be identified in the cation spectrum of the *E. coli* hydrophilic compounds (Figure S4). Fragments of these amino acids resulting from the loss of their carboxyl group (-COOH), as well as their hydroxyl group (-OH), could be detected. The peaks at m/z 18 (NH_4^+) and m/z 30 ($CH_2NH_2^+$) strongly indicate the presence of nitrogen-bearing compounds (e.g., Khawaja et al., 2019), and likely signify smaller amino acid fragments (Klenner et al., 2020a).

In cation mass spectra of the hydrophilic cell compounds of both bacteria (Figures 5, S4, and S6), protonated metabolic intermediates of glycolysis and the synthesis of serine can be identified, namely glyceraldehyde-3-phosphate ($C_3H_7O_6P^+$), phosphohydroxypyruvic acid ($C_3H_6O_7P^+$) at m/z 171, 185. Protonated 3-phosphoglycerate ($C_3H_7O_7P^+$) is detectable in the *E. coli* hydrophilic compounds at m/z 187. Protonated nicotinamide and nicotinic acid, two other metabolic intermediates known to be present within bacterial cells (Careri et al., 1996), can be identified at m/z 123 and 124, respectively, in hydrophilic compound spectra of both bacterial cultures. While these mass lines exhibit lower amplitudes than most of the amino acid derived species, a peak at m/z 105 is much stronger and can be assigned to the cell constituent choline (Figures 5 and S4). The *E. coli* hydrophilic compound spectrum shows the metabolic intermediate L- cysteine sulfinic acid (Leinweber and Monty, 1962) at m/z 154.

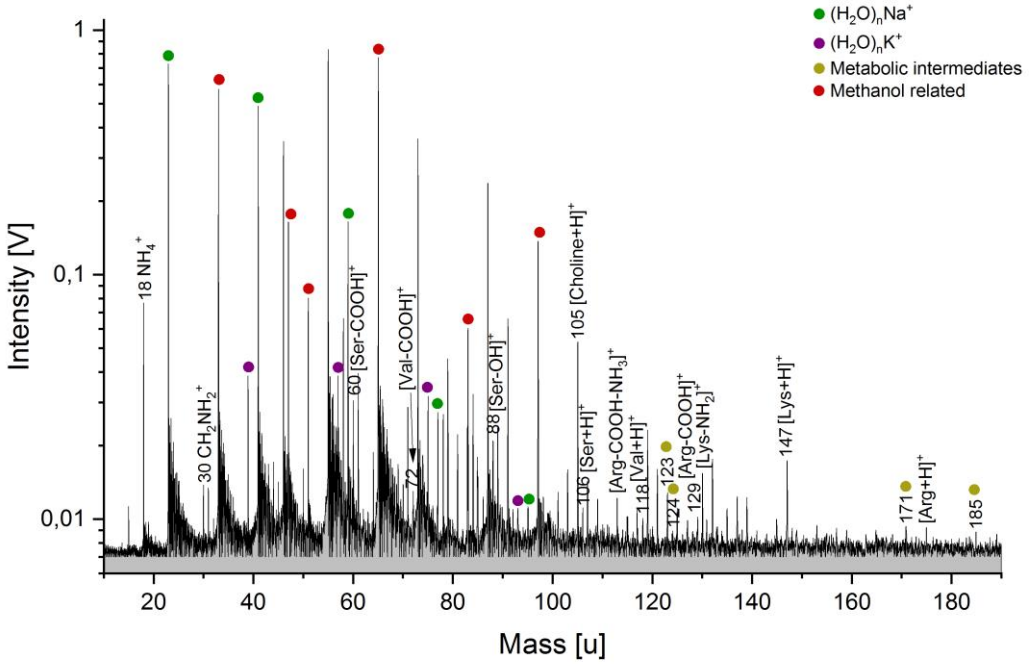

Figure 5: Baseline corrected cation mass spectrum (y-axis in logarithmic scale) of the hydrophilic cell compound from ~10^9 S. alaskensis cells, derived from the lipid extraction procedure (solution type iv). Amino acids as well as metabolites from the S. alaskensis cells are clearly detectable. The mass spectrum was recorded at a delay time of 6.2 µs and a laser intensity of 96.9 %.

In the anion mode (Figures 6 and S5), the most prominent peak can be observed at m/z 79, assigned to $[PO_3]^-$. This anion, together with deprotonated ribose at m/z 149, are remnants of the DNA's sugar-phosphate backbone. At lower amplitudes deprotonated nucleobases, fragments of the DNA molecule, can be

identified (Figure 6): adenine (m/z 134), guanine (m/z 150) and cytosine (m/z 110). As in the mass spectra of DNA, the fourth deprotonated nucleobase thymine interferes with a chlorine-water cluster peak from the matrix $(H_2O)_5Cl^-$ and thus can only be tentatively assigned to m/z 125. Deprotonated glycine (m/z 74) as well as deprotonated cadaverine (m/z 101), an intermediate of bacterial L-lysine catabolism (Ma et al., 2015), are also observable. Deprotonated glutamic acid (m/z 146) can be identified in the *S. alaskensis* hydrophilic compound spectrum (Figure S5).

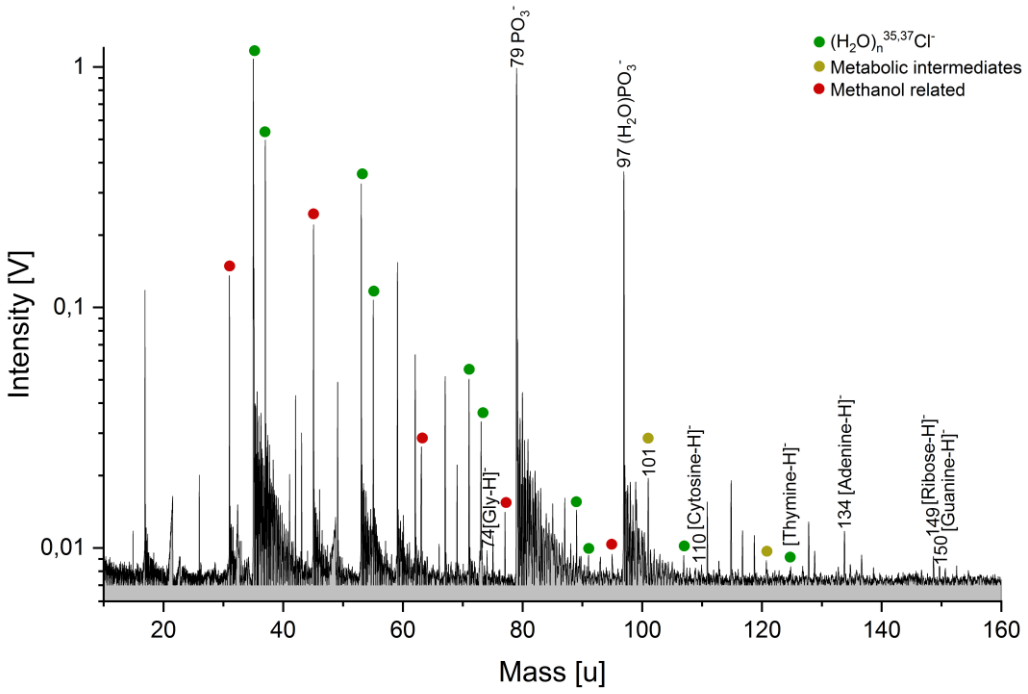

Figure 6: Section (m/z 10-160) of a baseline corrected anion mass spectrum (y-axis

in logarithmic scale) of the hydrophilic cell compounds from ~10^9 E. coli cells, derived from the lipid extraction procedure (solution type iv). Nucleobases (DNA fragments) as well as metabolites from the E. coli cells are clearly detectable. The mass spectrum was recorded at a delay time of 5.6 µs and a laser intensity of 96.2 %.

In cation and anion spectra of the hydrophilic cell compounds measured in matrices with increasing NaCl concentrations (solution type v), an increasing abundance of Na^+ or Cl^- related peaks, respectively, can be observed while peak amplitudes of protonated/deprotonated nucleobases, amino acids or metabolic intermediates decrease (Figure S6).

In high salinity ($\geq 10^{-2}$ M NaCl) solutions, amino acids are expected to form sodiated molecules rather than protonated molecules (Klenner et al., 2020b). Indeed, in cation mass spectra of the *E. coli* hydrophilic compounds, sodiated serine and trisodiated asparagine can be assigned to m/z 128 and 199, respectively, as shown in Figure S6. Deoxyribose can be identified as disodiated and trisodiated molecule at m/z 179 and 201, respectively. Sodiated nucleobases could not be identified. In anion mass spectra, $[PO_3]^-$, forming the most prominent peak in spectra of solution type iv, can still be identified, even if 10^{-1} M NaCl is added to the samples.

4 Discussion

In this work we have investigated the mass spectral appearances of bioessential molecules, namely DNA, lipids, and metabolic intermediates, extracted from two different bacteria, at impact speeds equivalent to those of ice grains ejected from an ocean-bearing icy moon and sampled in a spacecraft flyby. Characteristics of all investigated biosignatures are clearly detectable in the resulting mass spectra obtained from the analogue experiments. Any detection of these biosignature spectral signals would be a strong indication for organisms on an extraterrestrial world.

Numerical modeling of biogenic material and cells in the Enceladan vents, the moon's plume and its water-ice interface estimate cell densities at different locations in the subsurface ocean. Estimates of the expected cell densities in the plume, vents and bulk ocean water are summarized by Cable et al. (2021, Table 1). According to Steel et al. (2017) $\sim 10^9$ cells cm^{-3} may accumulate in the vents and $\sim 10^8$ cells cm^{-3} in the plume, whereas Porco (2017) estimates up to 10^7 cells mL^{-1} in the plume. The cell density at the ice ocean interface is estimated at 10^5 to 10^8 cells mL^{-1} by Russell et al. (2017). In the bulk ocean water cells will be diluted: Estimates range from 0.026 - 0.18 cells cm^{-3} (Ray et al., 2021), over 0.6 - 890 cells cm^{-3} (Vance et al., 2016), to 80 – 4250 cells cm^{-3} biomass potentially produced by methanogens (Steel et al. 2017). However, the estimated density values might increase by later enrichment as diluted water is transported to the surface in the case

of an organic film on top of the oceanic water table (Postberg et al., 2018a) where cell components decompose over time. Bursting gas bubbles at the water table efficiently enrich concentrations of organics in ice grains. This phenomenon is well observed in Earth's oceans and increases organic concentrations by 2-3 orders of magnitude (Russell et al., 2010; Burrows et al., 2014). This work focusses on the characterization of biosignatures in mass spectra rather than the determination of their detection limits. However, the used cell densities in our experiments (~10^9 cells mL^{-1}), although at the upper end of the estimates, still represent a plausible scenario for the Enceladan vent environment.

4.1 Deoxyribonucleic acid (DNA)

In positive and negative ion mode mass spectra of *E. coli* and *S. alaskensis* DNA, mass peaks of fragments deriving from both the nucleobases, and the phosphate-deoxyribose compounds could clearly be identified (Figures 2, 3).

Adenine, and guanine nucleobase molecules, as well as fragments resulting from the loss of ammonia, can be assigned to their respective mass peaks in both ion modes, whereas the molecular peak of cytosine can only be identified in the positive ion mode. The potential molecular peak of thymine overlaps (mass difference < 0.007 u) with a water cluster peak at m/z 127 and m/z 125 in positive and negative ion mode, respectively, and cannot be resolved with the available mass resolution

of the experimental setup (600 – 800 m/Δm). Its presence in the LILBID mass spectra, however, can be inferred indirectly, by the detection of its fragment [Thymine-CH_3] at m/z 111. Due to the ambiguity of the thymine molecular peak, and the sensitivity variations of our setup that result in nucleobase peaks with different intensities, the equal ratio of adenine to thymine and guanine to cytosine, cannot be clearly identified as a potential biosignature in the mass spectra of the water ice grains. We instead find that our setup is particularly sensitive to purine bases (adenine and guanine) compared to pyrimidine bases. In the anion mode, we can easily detect the most characteristic DNA fragments (deprotonated nucleobases) at 1 ppmw (Figure 3) and the detection limit probably lies below this concentration. In the cation mode, we infer that a concentration of ~50 ppmw is sufficient to identify protonated nucleobases.

DNA is quite water soluble and thus might not only be expected in a salt-poor organic layer on top of an icy moon's ocean, but also in the salt-rich bulk water phase. Although the salinity of Enceladus' subsurface ocean is expected to decrease the sensitivity of the impact ionization mass spectrometer to the mass spectral signals of DNA enclosed in salt-rich ice grains (Annesley, 2003; Piwowar et al., 2009; Klenner et al., 2020b), our experiments with DNA in salt-rich matrices (solution ii) show that deprotonated nucleobases, especially purines, can still be detected up to a NaCl concentration of 0.01 M (Figure 2). While an alien biochemistry might utilize a different set of nucleobases, this work demonstrates

the ability of impact induced ionization mass spectrometry to detect this class of biosignature molecules in ocean world relevant conditions.

4.2 Lipids

The surface microlayer at the water-atmosphere interface of terrestrial oceans contains microorganisms at high cell densities, as well as various hydrophobic compounds produced by the bacteria (Hardy, 1982; Franklin et al., 2005). In Enceladus' subsurface ocean hydrophobic compounds could partition into a tiny low-salinity organic layer on top of the water body as hypothesized by Postberg et al. (2018b). Thus, such compounds would probably enter the jets incorporated in salt-poor ice grains.

Both *E. coli* and *S. alaskensis* lipids as well as lipid fragments, such as fatty acids, were found to be clearly identifiable in anion mass spectra (Figure 4). In the *E. coli* lipid spectra, the ratio of odd- to even carbon number fatty acids (C_{14}-C_{20}) matches the spectral appearance of biotically produced fatty acid abundances predicted by Klenner et al. (2020b). Even carbon number fatty acids produce higher peak amplitudes compared to odd carbon number fatty acids, with C_{16} and C_{18} being most abundant. In *S. alaskensis* lipid spectra, similar abundances can be observed, with C_{15} in addition to C_{16} and C_{18}, being most abundant.

The observed lipid patterns in this work display differences to the fatty acids abundances expected from previously published literature. We observe a relatively high abundance of saturated fatty acids over the unsaturated fatty acid of the same carbon atom number (Figure 4). While C_{16} and C_{18} are indeed expected to be major in *E. coli* strain W3110, Mejía et al. (1999) observe unsaturated C_{16} and C_{18} to be more abundant relative to saturated C_{16} and C_{18}. Similarly for *S. alaskensis*, Kim et al. (2005) and Choi et al. (2010) report a higher relative abundance of unsaturated C_{18} over saturated $C_{18.}$ Additionally, the peak deriving from unsaturated C_{17} is expected to be major in *S. alaskensis* while saturated C_{15} and C_{16} are usually less pronounced. At this point we are unable to pinpoint the origin of the mismatches of our data with previously published literature. However, measuring a mixture of saturated along with unsaturated fatty acids at equimolar concentrations shows that relative abundances of fatty acids, independent of the degree of saturation, are accurately reflected in the acids' deprotonated molecular peaks in LILBID spectra (Figure S7).

In the subsurface ocean of Enceladus lipids deriving from the decay of the potential microorganisms, and other hydrophobic molecules could reside in the surface biofilm and could be detected in the ice grains upon entering the plume by SUDA- or ENIA-type instruments. In the biofilm, the lipids may be exposed to low or intermediate salt concentrations (Postberg et al., 2018a). Spectra recorded of lipids in 10^{-3} M sodium chloride solutions show that the strongest fatty acid peaks are still

clearly detectable. This is consistent with the results of Klenner et al. (2020b) which found fatty acids at intermediate salt concentrations to be detectable down to the ppm level. In Klenner et al. (2020b), fatty acids were also found to form sodiated dimers in saltwater matrices, at intermediate salt concentrations. As with nucleobases, an alien biochemistry might utilize different lipid carbon chain lengths, but this work demonstrates that the most prevalent molecules of this biomolecular class could be identified with impact induced ionization mass spectrometry.

4.3 Hydrophilic cell compounds

With the diversity of chemical compounds, the potential formation of charged molecules or fragments that might interfere with each other in the mass spectra, increases. Thus, in addition to the characterization of the mass spectral signals of single biosignatures (DNA, lipids), their identification within more complex mixtures, such as the hydrophilic cell compounds (from ~10^9 bacterial cells) analyzed in this work, is particularly relevant and represents a more realistic case for space missions to ocean moons.

In anion mass spectra of *E. coli* and *S. alaskensis* hydrophilic cell components, we clearly identify DNA-derived biosignatures, such as nucleobases, fragments thereof and phosphate moieties (Figure 6 and S5). Distinct signals of amino acids can be identified in the cation mode spectra (Figure 5, S4 and S6). Klenner et al. (2020a,

2020b) inferred amino acid detection limits in salt-poor and salt-rich solutions to be at the ppm or ppb level. The identification of amino acids and their relative abundances are promising approaches in the detection of biosignatures in icy moon environments (Davila and McKay, 2014; Klenner et al., 2020b). Amino acids have been proposed to decompose in hydrothermally active oceans at relatively short geologic time scales (<1 Myr, Truong et al., 2019). Thus, a detection of free amino acids even at the ppb level in Enceladus' subsurface ocean today would indicate them being recently produced and not relicts of primordial synthesis. Further metabolic intermediates of glycolysis and other metabolic pathways could be assigned in both ion modes. Additionally, the intracellular sodium, potassium, and chloride ions (Schultz et al., 1961, 1962) produced characteristic peaks in the mass spectra though these ions would be difficult to identify as cell-sourced in salt-rich ice grain mass spectra.

Positive ion mode spectra recorded with *E. coli* hydrophilic cell components in NaCl matrices with rising concentrations (solution v) show the formation of sodium- complexed adducts such as mono- and trisodiated amino acids, whereas chlorinated ions in the negative ion mode spectra are not observed. Thus, our results are in accordance with the findings of Klenner et al. (2020b) that amino acids are more easily detected in the cation mode and tend to form sodiated cations in NaCl solutions. The biosignatures are detectable in salt-rich background solutions up to 10^{-2} M NaCl, and $[PO_3]^-$ can even be detected in anion mass spectra when 10^{-1} M

NaCl is present. With the analysis of the hydrophilic cell compounds after lipid extraction we show that these characteristic biosignature molecules can still be identified in impact ionization mass spectra of ice grains containing complex mixtures including many hydrophilic cell compounds.

4.4 Comparison of Biosignatures from *E. coli* and *S. alaskensis*

Both *E. coli* and *S. alaskensis* have their own respective importance to our experiments. While the potential presence of *E. coli*-like mesophilic bacteria in Enceladus subsurface environment is questionable as they are very rare in unpolluted marine environments on Earth and susceptible to temperature fluctuations (Bonde, 1967; van Elsas et al., 2011), experiments conducted with such a highly researched model organism form a promising basis for further experiments and substantiate data interpretation with a wide range of publications (Blount, 2015; Cronan, 2014). *E. coli* bacteria have even recently been used in experiments simulating the effect of ejection into space, as occurs from Enceladus' plume as a reference for future research (Bywaters et al., 2020). Psychrophilic bacteria, such as *S. alaskensis*, are more likely to survive in the conditions of the icy moon environment due to their adaptation abilities to cold temperatures. As heterotrophs both bacteria would require a structured ecosystem including autotrophs capable of carbon fixation to provide organic carbon.

The identification of characteristic differences in the mass spectral appearance of biosignatures from *E. coli* and *S. alaskensis* helps to determine the sensitivity of the analogue experiments to species-specific characteristics, potentially linked to adaptations to their mesophilic (*E. coli*) and psychrophilic (*S. alaskensis*) lifestyles. We were able to clearly identify such differences in the mass spectra resulting from *E. coli* and *S. alaskensis* lipids and hydrophilic cell compounds. The DNA mass spectra of both bacteria show the same characteristic biosignatures due to the fact that we mainly identify the DNA building blocks that unite all terrestrial life.

A prominent distinction in the lipid abundances of the two bacteria is the high amplitude of the C_{15} peak in *S. alaskensis* lipid spectra at m/z 141. We also observe a common adaptation of psychrophilic microorganisms to cold temperatures: an increase in the ratio of (poly)unsaturated to saturated fatty acids in the membrane lipids (van Dooremalen and Ellers, 2010), i.e., a higher amount of unsaturated fatty acids within the bacterial lipids, is a mechanism of these bacteria to maintain membrane fluidity. We can clearly identify such a difference between mass spectra of *S. alaskensis* and *E. coli* lipids (Figure 4). In the *S. alaskensis* lipid spectra, we identified not only a higher amount but also more diverse unsaturated fatty acids. Analogous to *S. alaskensis*, potential psychrophilic bacteria located in the upper layers of an Enceladan subsurface ocean might have membranes composed of similar fatty acid ratios which would reside in the surface biofilm from where they could enter the plume.

In mass spectra of the hydrophilic cell compounds, especially the amino acid abundances are of interest for the distinction of the two bacteria, as the substitution of certain amino acids in proteins presents another common adaptation of bacteria to changes in environmental conditions. New findings suggest that specific amino acids prevail in cell cultures of *Colwellia psychrerythraea,* a psychrophilic bacterium, depending on the growth temperature and medium salinity, tested as independent factors and in combination (Mudge et al., 2021). Cultures grown at lower, subzero temperatures showed a significant enrichment in glutamic acid and valine and a depletion of aspartic acid and threonine, whereas samples grown under salt-rich conditions were enriched in alanine and again, reduced in asparagine. In accordance with the temperature gradient experiments, we do identify threonine only in mass spectra of the hydrophilic cell compounds of mesophilic *E. coli* cell cultures and not in the psychrophilic *S. alaskensis (*Figures S4 and 5), while we identify glutamic acid from *S. alaskensis* cultures but not from *E. coli* cultures (Figures 6 and S5). In our experiments, *S. alaskensis* was grown at 29 °C, thus these features cannot be related to active cold adaptation but presumably integral characteristics of the psychrophilic bacterium. Such temperature- and salinity dependent characteristics, e.g., a depletion of Asp with lower temperature and higher salinity, help identifying what to expect from mass spectral signals of potential microorganisms grown under the conditions of Enceladus' and Europa's

subsurface oceans. Thus, identifying the differences in characteristic mass spectral signals of the two bacteria is of great importance.

However, the similarities also bear valuable information as they pinpoint characteristics that unite bacterial life. In DNA spectra of both bacteria, we identify the same universal building blocks, the nucleobases and fragments of the deoxyribose-phosphate moieties (Figures 2 and 3). Additionally, we were able to detect characteristics of universal metabolic pathways, intermediates of glycolysis and serine synthesis, in cation spectra of the hydrophilic cell compounds of both bacteria. While an alien biochemistry might utilize different nucleobases, the efficacy of impact induced ionization mass spectrometry in identifying these patterns means this technique is able to test ocean world environments for this class of biosignature molecules.

5 Conclusions and outlook

The ability of the LILBID technique to accurately simulate mass spectra of chemical compounds enclosed in water ice grains and detected by impact ionization mass spectrometers on-board future space missions was applied to predict characteristic mass spectral signals of bacterial cell components, namely DNA, lipids, and metabolic intermediates. Mass spectral characteristics of these molecules could be clearly identified in flight mass spectra even if the biosignatures

were encased in ice grains with significant amounts of salts. Two different bacterial species also presented unique biosignature fingerprints, indicating that this technique might also distinguish between different types of microorganisms, although further work is needed. The impact ionization process in space, simulated in the LILBID setup, would create charged molecules, or fragments from these biogenic substances, that could be unambiguously detected by SUDA- or ENIA-type mass spectrometers on future space probes.

From our experimental results, we can infer recommendations for future space probes that will sample the ice grains ejected from icy moons, in terms of both sensitivity of the on-board mass spectrometer and the impact speed of the ice grains onto its metal target. The investigations in this work demonstrate, together with previous results (Klenner et al., 2020a, 2020b), that mass spectral analysis in both anion and cation mode is needed to detect the complete range of biosignatures investigated in our experiments: metabolic intermediates, while detectable in both ion modes, show a higher sensibility to cation mode detection, while DNA is preferentially, and lipids exclusively, detected in anion mode. In their respective optimal ion mode, all investigated biosignatures are detectable down to the ppm-level, and some of them clearly below. Due to more efficient ion detectors, detection limits of space instrument are expected to be improved by one to two orders of magnitude compared to our laboratory setup.

Combinations of delay times and laser intensities can be correlated to different impact speeds of ice grains onto metal targets of SUDA-like detectors in space (Klenner et al., 2019). Thus, with the settings used in our analogue experiments, we can recommend optimal encounter velocities that result in the most distinguished peaks of the investigated molecules in the mass spectra. LILBID experiments of Klenner et al. (2020a, 2020b), as well as computer simulations by Jaramillo-Botero et al. (2021) suggest optimal encounter velocity ranges of 4-6 km/s for amino acids and fatty acids. From our experiments, we infer optimal encounter velocities of 4-8 km/s for DNA, 3-6 km/s for lipids and 4-7 km/s for metabolic intermediates, respectively. Thus, in accordance with Klenner et al. (2020a, 2020b) and Jaramillo-Botero et al. (2021), we derive at the same recommended velocity window of 4-6 km/s for the optimal detection of all investigated biosignatures which is in the range of the expected flyby speeds of the Europa Clipper spacecraft (typically 4–5 km/s). However, it should be noted that slightly higher impact speeds - in the order of 7 – 10 km/s - might be useful to complement spectra recorded at lower speeds to provoke a more abundant creation of characteristic fragments, albeit on the cost of lower signals from parent molecules.

In the future, we will perform experiments to determine to what extent characteristic biosignatures of whole cells - without any preceding extraction method - can be identified in impact ionization mass spectra. Additionally, we plan to determine which mass spectral characteristics of other metabolisms or

mechanisms that might enable survival under the conditions of the Enceladan or Europan subsurface ocean, e.g., methanogenesis, chemoautotrophy, sulfate reduction or a tolerance to radiation, can be detected in the analogue experiments. In this context, we aim to investigate the effects of direct contact with oxidants and ionizing radiation on the preservation of different biosignatures. By extending the range of biosignatures from a number of different species exposed to different conditions we aim to maximize the information that can be gained from future data recorded by SUDA-type mass spectrometers on space missions to ocean worlds.

Acknowledgements

Authors acknowledge the collaboration of the Planetary Sciences and Remote Sensing group at Freie Universität Berlin and the Leibniz Institute of Surface Engineering (IOM, Leipzig) in the framework of their joint Icy Micro Particles (IMP) laboratory. We thank Eberhard Klauck and Ben J. Lambeck (Freie Universität Berlin) for preparing some of the DNA samples, Andreas Elsäßer and David Burr (Freie Universität Berlin) for culturing *E. coli* cells as well as Alex Price (The Open University) for culturing *S. alaskensis* cells. We also thank Dr. Ales Charvat for help and assistance with the laser desorption MS setup. Intensive discussions on the lipid spectra with Geraint (Taff) Morgan (The Open University) are warmly acknowledged. Some of this work was conducted at the Jet Propulsion

Laboratory, California Institute of Technology, under a contract with the National Aeronautics and Space Administration (80NM0018D0004). Reference herein to any specific commercial product, process, or service by trade name, trademark, manufacturer, or otherwise, does not constitute or imply its endorsement by the United States Government or the Jet Propulsion Laboratory, California Institute of Technology.

Author Disclosure Statement

No competing financial interests exist.

Funding Information

The research leading to these results received financial support from the European Research Council (ERC) under the European Union's Horizon 2020 research and innovation program (ERC Consolidator Grant 724908-Habitat OASIS).

References

Ames GF (1968) Lipids of *Salmonella typhimurium* and *Escherichia coli*: structure and metabolism. *J Bacteriol* 95:833–843.

Annesley TM (2003) Ion suppression in mass spectrometry. *Clin Chem* 49:1041–1044.

Belousov A, Miller M, and Continetti R, et al. (2021) Sampling Accelerated Micron Scale Ice Particles with a Quadrupole Ion Trap Mass Spectrometer. *J Am Soc Mass Spectrom* 32:1162–1168.

Bertani G (1951) Studies on lysogenesis I: the mode of phage liberation by lysogenic Escherichia coli. *J Bacteriol* 62:293-300.

Bezdek HF, and Carlucci AF (1972) Surface concentrations of marine bacteria 1. *Limnol Oceanogr* 17:566-569.

Bligh EG, and Dyer WJ (1959) A rapid method of total lipid extraction and purification. *Can J Biochem Physiol* 37:911–917.

Blount ZD (2015) The unexhausted potential of *E. coli*. *eLife 4:*e05826.

Bonde GJ (1967) Pollution of a marine environment. *J Water Pollut Control Fed* R:45-63.

Bouquet A, Glein CR, and Waite JH (2019) How Adsorption Affects the Gas–Ice Partitioning of Organics Erupted from Enceladus. *ApJ* 873:28.

Bowden SA, Parnell J, and Burchell MJ (2009) Survival of organic compounds in ejecta from hypervelocity impacts on ice. *Int J Astrobiology* 8:19–25.

Brown ME, and Hand KP (2013) Salts and radiation products on the surface of Europa. *AJ* 145:110.

Burchell MJ, Bowden SA, and Cole M, et al. (2014) Survival of organic materials in hypervelocity impacts of ice on sand, ice, and water in the laboratory. *Astrobiology* 14:473–485.

Burrows SM, Ogunro O, and Frossard AA, et al. (2014) A physically based framework for modeling the organic fractionation of sea spray aerosol from bubble film Langmuir equilibria. *Atmos Chem Phys* 14:13601–13629.

Bywaters K, Stoker CR, and Batista Do Nascimento N, et al. (2020) Towards Determining Biosignature Retention in Icy World Plumes. *Life (Basel)* 10:40.

Careri M, Cilloni R, and Lugari MT, et al. (1996) Analysis of water-soluble vitamins by high-performance liquid chromatography–particle beam-mass spectrometry. *Anal Commun* 33:159–162.

Cavicchioli R, Ostrowski M, and Fegatella F, et al. (2003) Life under nutrient limitation in oligotrophic marine environments: an eco/physiological perspective of *Sphingopyxis alaskensis* (formerly *Sphingomonas alaskensis*). *Microb Ecol* 45:203–217.

Charvat A, and Abel B (2007) How to make big molecules fly out of liquid water: applications, features and physics of laser assisted liquid phase dispersion mass spectrometry. *Phys Chem Chem Phys* 9:3335–3360.

Choi JH, Kim MS, and Jung MJ, et al. (2010) *Sphingopyxis soli* sp. nov., isolated from landfill soil. *Int J Syst Evol Microbiol* 60:1682–1686.

Cockell CS, Bush T, and Bryce C, et al. (2016) Habitability: A Review. *Astrobiology* 16:89–117.

Cronan JE (2014) *Escherichia coli* as an Experimental Organism. *eLS* 2014.

Davila AF, and McKay CP (2014) Chance and necessity in biochemistry: implications for the search for extraterrestrial biomarkers in Earth-like environments. *Astrobiology* 14:534–540.

Duncan JH, Lennarz WJ, and Fenselau CC (1971) Mass spectral analysis glycerophospholipids. *Biochemistry* 10:927–932.

Eguchi M, Nishikawa T, and MacDonald K, et al. (1996) Responses to stress and nutrient availability by the marine ultramicrobacterium *Sphingomonas* sp. strain RB2256. *Appl Environ Microbiol* 62:1287–1294.

Eguchi M, Ostrowski M, and Fegatella F, et al. (2001) *Sphingomonas alaskensis* strain AFO1, an abundant oligotrophic ultramicrobacterium from the North Pacific. *Appl Environ Microbiol* 67:4945–4954.

Fisher CR, Price MC, and Burchell MJ (2021) Salt grains in hypervelocity impacts in the laboratory: Methods to sample plumes from the ice worlds Enceladus and Europa. *Meteorit Planet Sci* 56:1652–1668.

Flemming HC, and Wuertz S (2019) Bacteria and archaea on Earth and their abundance in biofilms. *Nat Rev Microbiol* 17:247–260.

Franklin R, and Gosling R (1953) Molecular Configuration in Sodium Thymonucleate. *Nature* 171:740–741.

Franklin MP, McDonald IR, and Bourne DG, et al. (2005) Bacterial diversity in the bacterioneuston (sea surface microlayer): the bacterioneuston through the looking glass. *Environ Microbiol* 7:723-736.

Georgiou CD, and Deamer DW (2014) Lipids as universal biomarkers of extraterrestrial life. *Astrobiology* 14:541–549.

Hand KP, Carlson RW, and Chyba CF (2007) Energy, chemical disequilibrium, and geological constraints on Europa. Astrobiology 7:1006–1022.

Hansen CJ, Esposito L, and Stewart AIF, et al. (2006) Enceladus' water vapor plume. *Science* 311:1422–1425.

Hardy, JT (1982) The sea surface microlayer: biology, chemistry and anthropogenic enrichment. *Prog Oceanogr* 11:307-328.

Hillier JK, Sestak S, and Green SF, et al. (2009) The production of platinum-coated silicate nanoparticle aggregates for use in hypervelocity impact experiments. *Planet Space Sci* 57:2081–2086.

Hillier JK, Sternovsky Z, and Kempf S, et al. (2018) Impact ionisation mass spectrometry of platinum-coated olivine and magnesite-dominated cosmic dust analogues. *Planet Space Sci* 156:96–110.

Hoppa GV, Tufts BR, Greenberg R, and Geissler PE (1999) Formation of Cycloidal Features on Europa. *Science* 285:1899–1902.

Howell SM, and Pappalardo RT (2020) NASA's Europa Clipper-a mission to a potentially habitable ocean world. *Nat commun* 11:1311.

Hudson JS, Eberle JF, and Vachhani RH, et al. (2012) A unified mechanism for abiotic adenine and purine synthesis in formamide. *Angew Chem Int Ed* 51:5134–5137.

Jaramillo-Botero A, Cable ML, and Hofmann AE, et al. (2021) Understanding Hypervelocity Sampling of Biosignatures in Space Missions. *Astrobiology* 21:421–442.

Jia X, Kivelson MG, and Khurana KK, et al. (2018) Evidence of a plume on Europa from Galileo magnetic and plasma wave signatures. *Nat Astron* 2:459–464.

Kazemi B, New JS, and Golozar M, et al. (2021) Method for detecting and quantitating capture of organic molecules in hypervelocity impacts. *Methodsx* 8:101239.

Kempf S, Altobelli N, and Briois C, et al. (2014) SUDA: A Dust Mass Spectrometer for Compositional Surface Mapping for a Mission to Europa. *EPSC* 9:EPSC2014-229.

Khawaja N, Postberg F, and Hillier J, et al. (2019) Low-mass nitrogen-, oxygen-bearing, and aromatic compounds in Enceladean ice grains. *Mon Not R Astron Soc* 489:5231–5243.

Kim MK, Im Wan T, and Ohta H, et al. (2005) *Sphingopyxis granuli* sp. nov., a beta-glucosidase-producing bacterium in the family Sphingomonadaceae in alpha-4 subclass of the Proteobacteria. *J Microbiol* 43:152-157.

Kleinekofort W, Avdiev J, and Brutschy B (1996a) A new method of laser desorption mass spectrometry for the study of biological macromolecules. *Int J Mass Spectrom Ion Processes* 152:135–142.

Kleinekofort W, Pfenninger A, and Plomer T, et al. (1996b) Observation of noncovalent complexes using laser-induced liquid beam ionization/desorption. *Int J Mass Spectrom Ion Processes* 156:195–202.

Klenner F, Postberg F, and Hillier J, et al. (2019) Analogue spectra for impact ionization mass spectra of water ice grains obtained at different impact speeds in space. *Rapid commun Mass Spectrom* 33:1751–1760.

Klenner F, Postberg F, and Hillier J, et al. (2020a) Analog Experiments for the Identification of Trace Biosignatures in Ice Grains from Extraterrestrial Ocean Worlds. *Astrobiology* 20:179–189.

Klenner F, Postberg F, and Hillier J, et al. (2020b) Discriminating Abiotic and Biotic Fingerprints of Amino Acids and Fatty Acids in Ice Grains Relevant to Ocean Worlds. *Astrobiology* 20:1168–1184.

Klenner F, Umair M, and Walter SHG, et al. (under review) Developing a Laser Induced Liquid Beam Ion Desorption Spectral Database as Reference for Spaceborne Mass Spectrometers. *Earth and Space Science*.

Krokan HE, Drabløs F, and Slupphaug G (2002) Uracil in DNA--occurrence, consequences and repair. *Oncogene* 21:8935–8948.

Kumar S, Chinnusamy V, and Mohapatra T (2018). Epigenetics of modified DNA bases: 5-methylcytosine and beyond. *Front Genet* 9*:*640.

Langworthy TA (1982) Lipids of Bacteria Living in Extreme Environments. In Current Topics in Membranes and Transport: Membrane Lipids of Prokaryotes, edited by F. Bronner, and A. Kleinteller. Academic Press, pp 45–77.

Leinweber FJ, and Monty KJ (1962) The metabolism of cysteine sulfinic acid in *Escherichia coli*. *Biochim Biophys Acta* 63:171–179.

Ligier N, Poulet F, and Carter J, et al. (2016) VLT/SINFONI observations of Europa: New insights into the surface composition. *AJ* 151:163.

López-Lara IM, and Geiger O (2017) Bacterial lipid diversity. *Biochim Biophys Acta Mol Cell Biol Lipids* 1862:1287-1299.

Ma W, Cao W, and Zhang H, et al. (2015) Enhanced cadaverine production from L-lysine using recombinant *Escherichia coli* co-overexpressing CadA and CadB. *Biotechnol Lett* 37:799–806.

MacFaddin JF (1985) Media for isolation, cultivation, identification, maintenance of medical bacteria, Williams & Wilkins, Baltimore Md, 1.

Mejía R, Gómez-Eichelmann MC, and Fernández MS (1999) *Escherichia coli* membrane fluidity as detected by excimerization of dipyrenylpropane: sensitivity to the bacterial fatty acid profile. *Arch Biochem Biophys* 368:156-160.

Mitri G, Postberg F, and Soderblom JM, et al. (2018) Explorer of Enceladus and Titan (E2T): Investigating ocean worlds' evolution and habitability in the solar system. *Planet Space Sci* 155:73–90.

Mudge MC, Nunn BL, and Firth E, et al. (2021) Subzero, saline incubations of *Colwellia psychrerythraea* reveal strategies and biomarkers for sustained life in extreme icy environments. *Environ Microbiol* 23:3840–3866.

New JS, Mathies RA, and Price MC, et al. (2020) Characterizing organic particle impacts on inert metal surfaces: Foundations for capturing organic molecules during hypervelocity transits of Enceladus plumes. *Meteorit Planet Sci* 55:465–479.

Oursel D, Loutelier-Bourhis C, and Orange N, et al. (2007) Lipid composition of membranes of Escherichia coli by liquid chromatography/tandem mass spectrometry using negative electrospray ionization. *Rapid commun mass spectrom* 21:1721–1728.

Piwowar AM, Lockyer NP, and Vickerman JC (2009) Salt effects on ion formation in desorption mass spectrometry: an investigation into the role of alkali chlorides on peak suppression in time-of-flight-secondary ion mass spectrometry. *Anal Chem* 81:1040–1048.

Poindexter JS (1981) Oligotrophy. In Advances in Microbial Ecology, edited by M. Alexander, Springer US, Boston, pp 63–89.

Porco CC, Helfenstein P, and Thomas PC, et al. (2006) Cassini observes the active south pole of Enceladus. *Science* 311:1393–1401.

Porco CC, Dones L, and Mitchell C (2017) Could It Be Snowing Microbes on Enceladus? Assessing Conditions in Its Plume and Implications for Future Missions. *Astrobiology* 17:876–901.

Postberg F, Kempf S, and Hillier JK, et al. (2008) The E ring in the vicinity of Enceladus: II. Probing the moon's interior – the composition of E-ring particles. *Icarus* 193.

Postberg F, Kempf S, and Schmidt J, et al. (2009) Sodium salts in E-ring ice grains from an ocean below the surface of Enceladus. *Nature* 459:1098–1101.

Postberg F, Grün E, and Horanyi M, et al. (2011) Compositional mapping of planetary moons by mass spectrometry of dust ejecta. *Planet Space Sci* 59:1815–1825.

Postberg F, Khawaja N, and Abel B, et al. (2018a) Macromolecular organic compounds from the depths of Enceladus. *Nature* 558:564–568.

Postberg F, Clark RN, and Hansen CJ, et al. (2018b) Plume and surface composition of Enceladus. In Enceladus and the Icy Moons of Saturn, edited by P.M. Schenk, R.N. Clark, C.J.A. Howet, A.J. Verbiscer, and J.H. Waite, University of Arizona Press, Tucson, AZ, pp 129–162.

Reh K, Spilker L, and Lunine JI, et al. (2016) Enceladus Life Finder: The search for life in a habitable Moon. *IEEE AeroConf*, pp 1–8.

Reiss CW, Xiong Y, and Strobel SA (2017) Structural Basis for Ligand Binding to the Guanidine-I Riboswitch. *Structure* 25:195–202.

Roth L, Saur J, and Retherford KD, et al. (2014) Transient water vapor at Europa's south pole. *Science* 343:171–174.

Russell LM, Hawkins LN, and Frossard AA, et al. (2010) Carbohydrate-like composition of submicron atmospheric particles and their production from ocean bubble bursting. *PNAS* 107:6652–6657.

Russell MJ, Barge LM, and Bhartia R, et al. (2014) The drive to life on wet and icy worlds. *Astrobiology* 14:308–343.

Russell MJ, Murray AE, and Hand KP (2017) The Possible Emergence of Life and Differentiation of a Shallow Biosphere on Irradiated Icy Worlds: The Example of Europa. *Astrobiology* 17:1265–1273.

Salter TL, Magee BA, and Waite JH, et al. (2022) Mass Spectrometric Fingerprints of Bacteria and Archaea for Life Detection on Icy Moons. *Astrobiology* 22:143–157.

Schultz SG, and Solomon AK (1961) Cation transport in *Escherichia coli.* I. Intracellular Na and K concentrations and net cation movement. *J Gen Physiol* 45:355–369.

Schultz SG, Epstein W, and Goldstein DA (1962) Cation transport in *Escherichia coli*. III. Potassium fluxes in the steadystate. *J Gen Physiol* 46:343–353.

Schut F, de Vries EJ, and Gottschal JC, et al. (1993). Isolation of typical marine bacteria by dilution culture: growth, maintenance, and characteristics of isolates under laboratory conditions. *Appl Environ Microbiol* 59:2150-2160.

Schut F, Gottschal JC, and Prins RA (1997). Isolation and characterisation of the marine ultramicrobacterium *Sphingomonas* sp. strain RB2256. *FEMS Microbiol. Rev* 20:363-369.

Singer SJ, and Nicolson GL (1972) The fluid mosaic model of the structure of cell membranes: Cell membranes are viewed as two-dimensional solutions of oriented globular proteins and lipids. *Science* 175:720–731.

Sparks WB, Hand KP, and McGrath MA, et al. (2016) Probing for evidence of plumes on Europa with HST /STIS. *ApJ* 829:121.

Spencer JR, Pearl JC, and Segura M, et al. (2006) Cassini encounters Enceladus: background and the discovery of a south polar hot spot. *Science* 311:1401–1405.

Srama R, Ahrens TJ, and Altobelli N, et al. (2004) The Cassini Cosmic Dust Analyzer. *Space Sci Rev* 114:465–518.

Srama R, Woiwode W, and Postberg F, et al. (2009) Mass spectrometry of hyper-velocity impacts of organic micrograins. *Rap Commun Mass Spectrom* 23:3895–3906.

Srama R, Postberg F, and Henkel H, et al. (2015) Enceladus Icy Jet Analyzer (ENIJA): Search for life with a high resolution TOF-MS for in situ characterization of high dust density regions. *EPSC* EPSC2015-769.

Steel EL, Davila A, and McKay CP (2017) Abiotic and Biotic Formation of Amino Acids in the Enceladus Ocean. *Astrobiology* 17:862–875.

Summons RE, Albrecht P, and McDonald G, et al. (2008) Molecular Biosignatures. *Space Sci Rev* 135:133-159.

Taj MK, Zohra S, and Ling JX, et al. (2014). *Escherichia coli* as a model organism. *Int J Eng Res Technol* 3:1-8.

Thomas PC, Tajeddine R, and Tiscareno MS, et al. (2016) Enceladus's measured physical libration requires a global subsurface ocean. *Icarus* 264:37–47.

Trumbo SK, Brown ME, and Hand KP (2019) Sodium chloride on the surface of Europa. *Sci Ad*v 5, eaaw7123.

Truong N, Monroe AA, and Glein CR, et al. (2019) Decomposition of amino acids in water with application to in-situ measurements of Enceladus, Europa and other hydrothermally active icy ocean worlds. *Icarus* 329:140-147.

van Dooremalen C, and Ellers J (2010) A moderate change in temperature induces changes in fatty acid composition of storage and membrane lipids in a soil arthropod. *J Insect Physiol* 56:178–184.

van Elsas JD, Semenov AV, and Costa R, et al. (2011) Survival of *Escherichia coli* in the environment: fundamental and public health aspects. *ISME* J 5:173–183.

Waksman SA, and Carey CL (1933) Role of Bacteria in Decomposition of Plant and Animal Residues in the Ocean. *Expl Biol Med* 30:526–527.

Watson JD, and Crick FH (1953) Molecular structure of nucleic acids; a structure for deoxyribose nucleic acid. *Nature* 171:737–738.

Wiederschein F, Vöhringer-Martinez E, and Beinsen A, et al. (2015) Charge separation and isolation in strong water droplet impacts. *Phys Chem Chem Phys* 17:6858–6864.

Wilkins M, Stokes A, and Wilson H (1953) Molecular Structure of Nucleic Acids: Molecular Structure of Deoxypentose Nucleic Acids. *Nature* 171:738–740.

Wirsen CO, Jannasch HW, and Wakeham SG, et al. (1986) Membrane lipids of a psychrophilic and barophilic deep-sea bacterium. *Curr Microbiol* 14:319–322.

Zeugin JA and Hartley JL, (1985) Ethanol precipitation of DNA. *Focus* 7:1-2.

Zhang Y, Ren G, and Buss J, et al. (2020) Enhancing colorimetric loop-mediated isothermal amplification speed and sensitivity with guanidine chloride. *BioTechniques* 69:178–185.

Supplementary Information (SI)

Supplementary Information S1: DNA extraction using the ethanol-precipitation method

DNA can be extracted from bacterial cells using an ethanol-precipitation method (Zeugin & Hartley 1985). The corresponding protocol involves incubating the bacterial cells in water, sodium acetate and ethanol for 15min at room temperature. During the incubation in ethanol, DNA precipitates from the solution. To collect the precipitate, the solution is then centrifuged at high speed, yielding a supernatant and a DNA pellet. After discarding the supernatant, the DNA pellet is rinsed with 70% ethanol and centrifuged for 15min. The ethanol is then removed via evaporation and the DNA pellet is dissolved in H_2O.

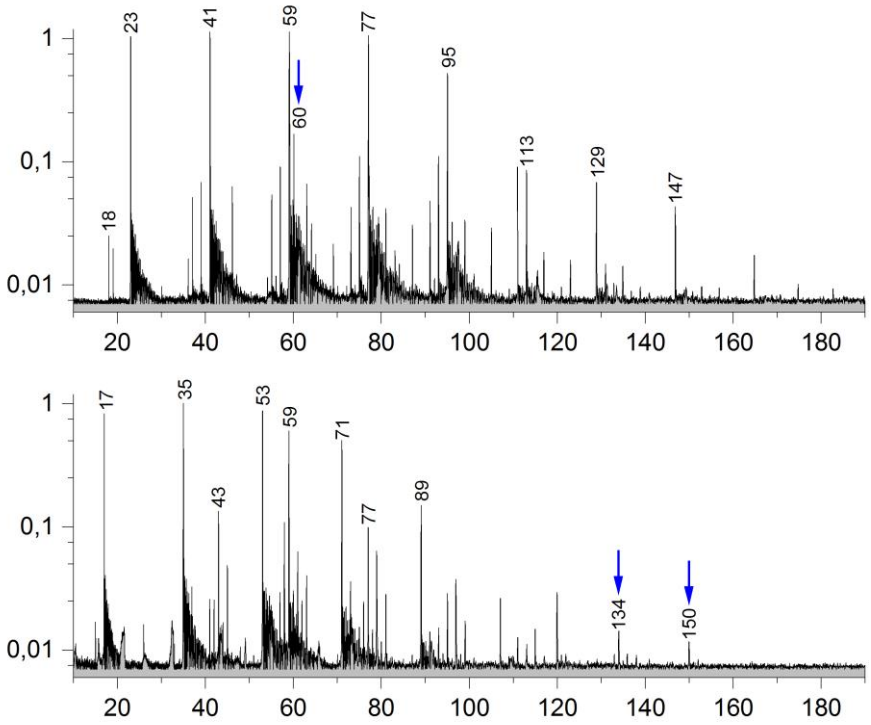

Figure S1: Cation (top) and anion (bottom) spectra of E. coli DNA (14 ppmw) in H_2O extracted with the ethanol-precipitation method, as described in Supplementary Information S1. m/z 60 in the cation spectrum derives from the DNA. Deprotonated nucleobases adenine and guanine are observed in the anion spectrum at m/z 134 and 150. No nucleobases are observed in the cation spectrum at the given concentration.

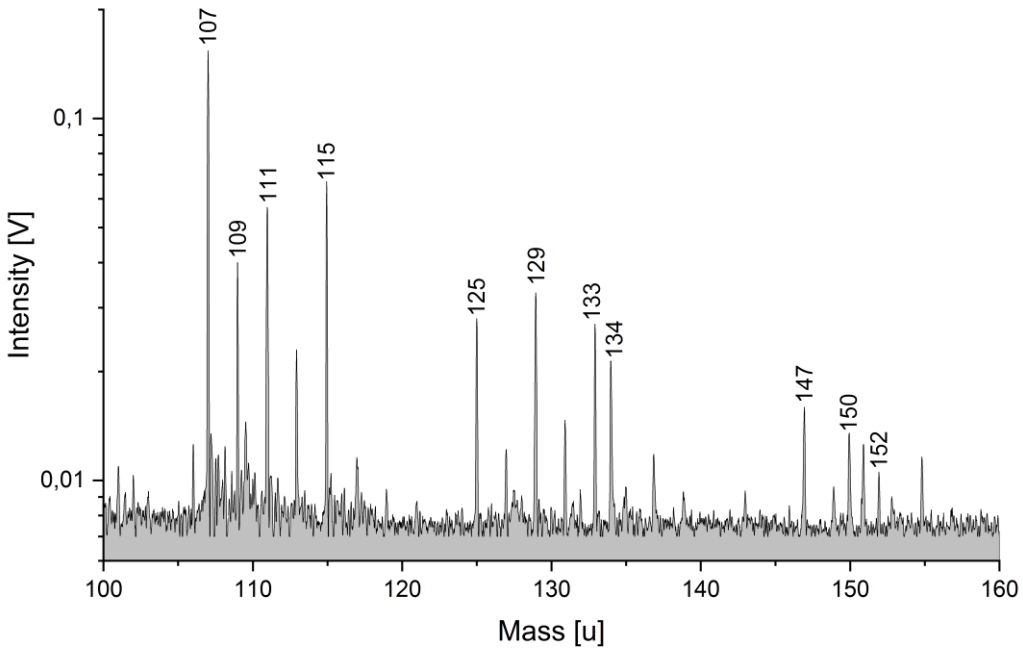

Figure S2: Section (m/z 100 - 160) of a baseline corrected anion mass spectrum (y-axis in logarithmic scale) of E. coli DNA (~100 ppmw) dissolved in a 0.01 M NaCl solution. Deprotonated adenine and guanine molecules are still detectable (m/z 134 and 150), even if significant NaCl concentrations are present. The mass spectrum was recorded at a delay time of 6.0 µs and a laser intensity of 97.3 %.

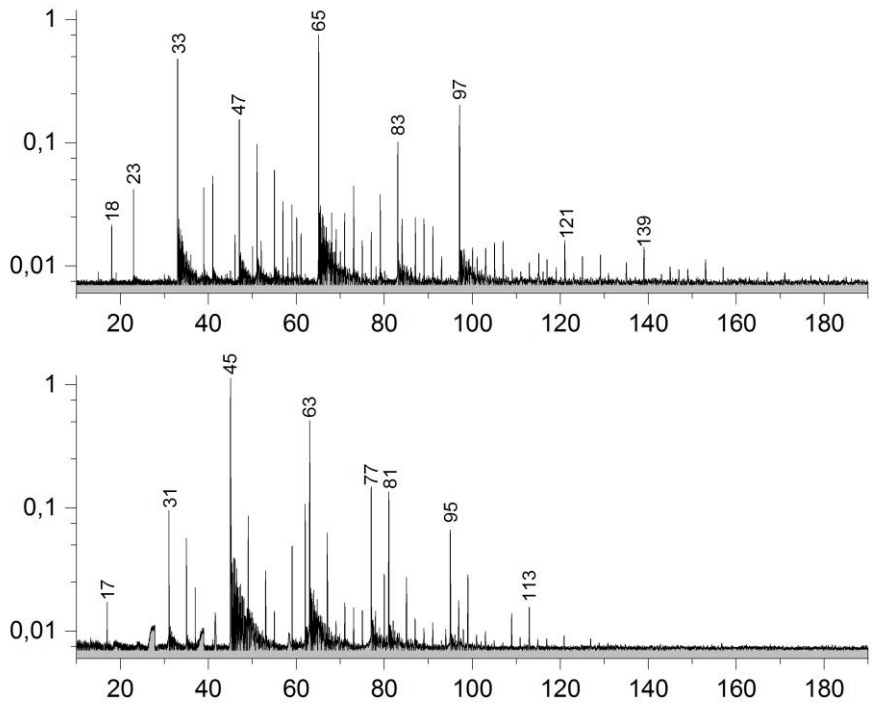

Figure S3: Cation (top) and anion (bottom) mass spectra (y-axis in logarithmic scale) of a methanol:water (1:1 vol.) solution. The mass spectra were recorded at delay times of 6.0 and 5.9 µs, respectively, and each at a laser intensity of 97.7 %.

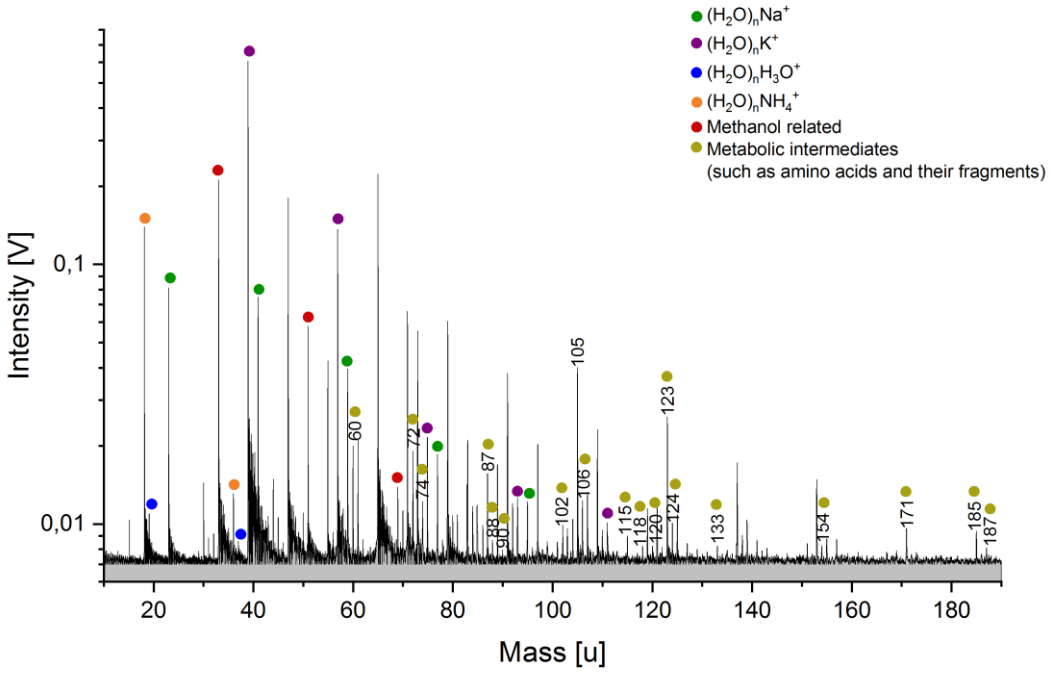

Figure S4: Baseline corrected cation mass spectrum (y-axis in logarithmic scale) of the aqueous phase from ~10^9 E. coli cells, derived from the lipid extraction procedure (solution type iv). Amino acids as well as other metabolites from the E. coli cells are clearly detectable. See main text (section 3.3) for further explanation. The mass spectrum was recorded at a delay time of 5.6 µs and a laser intensity of 96.2 %.

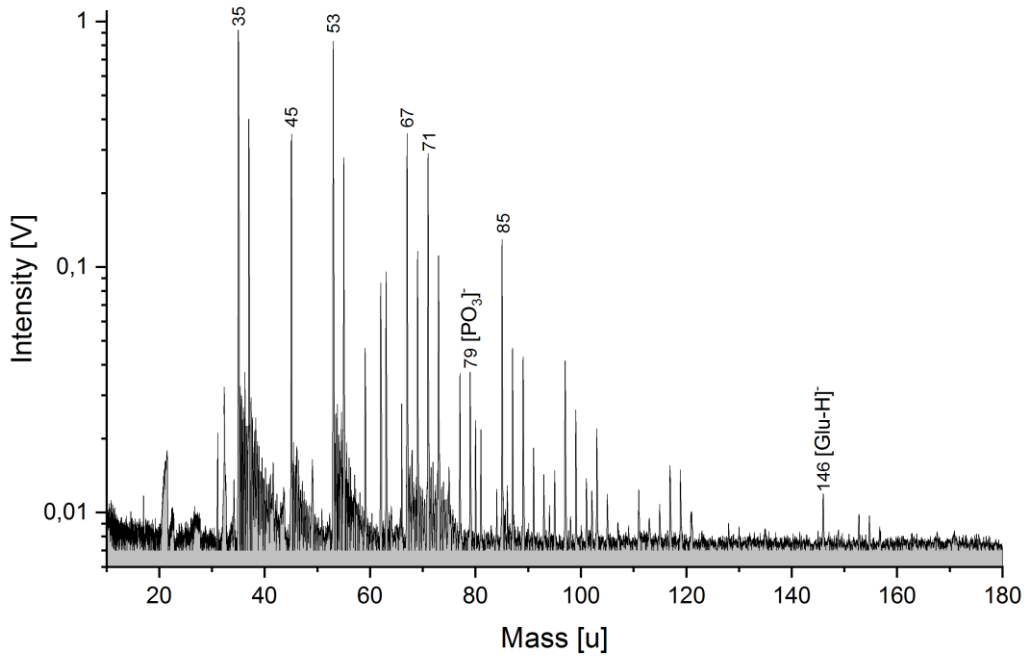

Figure S5: Baseline corrected anion mass spectrum (y-axis in logarithmic scale) of the aqueous phase from ~10^9 S. alaskensis cells, derived from the lipid extraction procedure (solution type iv). $[PO_3]^-$ derived from the DNA's phosphate-sugar backbone as well as glutamic acid (Glu) are clearly detectable. The mass spectrum was recorded at a delay time of 6.0 µs and a laser intensity of 98.5 %.

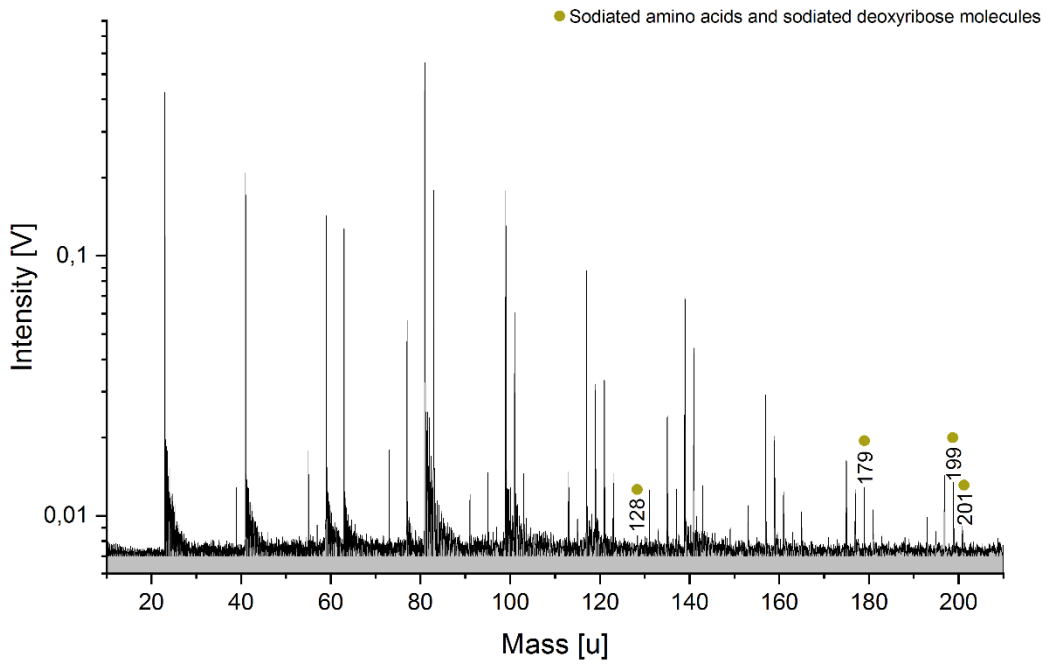

Figure S6: Baseline corrected cation mass spectrum (y-axis in logarithmic scale) of the E. coli aqueous phase (from ~10^9 cells) after adding 10^{-2} M NaCl to the sample. Sodiated molecules of serine (Ser), asparagine (Asn) and deoxyribose are identifiable (yellow dots). Unlabeled peaks are NaCl related. The mass spectrum was recorded at a delay time of 5.6 µs and a laser intensity of 96.2 %.

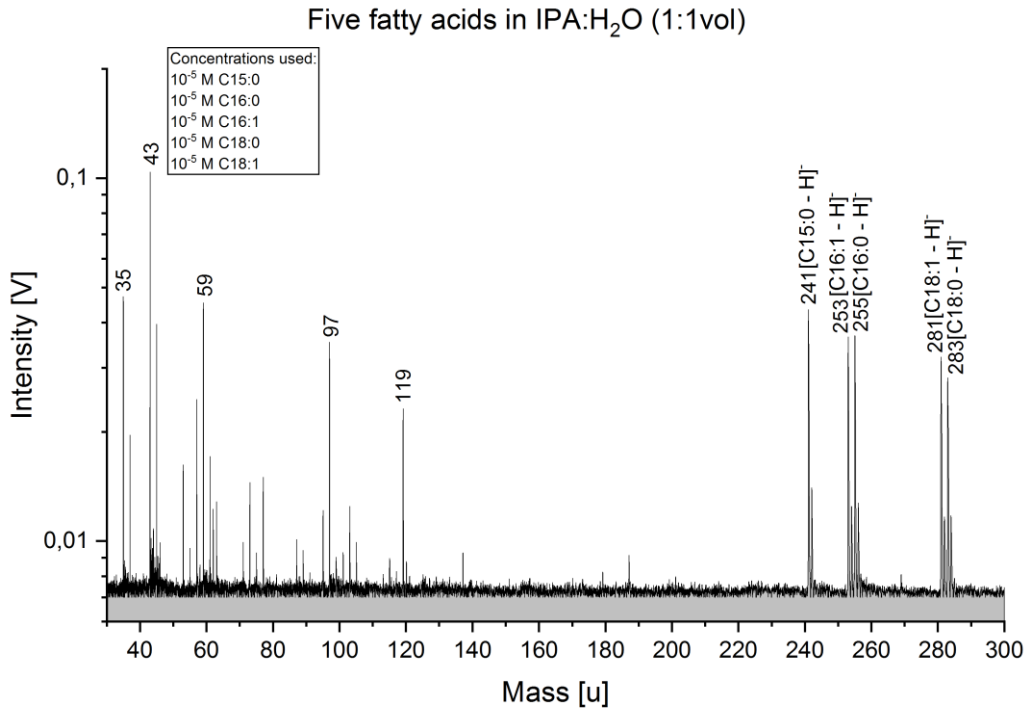

Figure S7: Baseline corrected anion mass spectrum of saturated as well as unsaturated fatty acids at equimolar concentrations (10^{-5} M) together in a matrix of water:isopropanol (50%vol each). Deprotonated fatty acid peaks are nearly equally high. A slight decrease with increasing carbon number can be observed, probably due to the fatty acids' increasing poor solubilities.